

Bachelorarbeit

von cand. aer. Mohamed Anes Asmi

**Development of a testing framework for  
evaluation of an aircraft engine controller**

November 2023

Bachelorarbeit

von cand. aer. Mohamed Anes Asmi

**Development of a testing framework for evaluation  
of an aircraft engine controller**

November 2023

betreut von

Prof. Dr.-Ing. Philipp Hartmann

mitbetreut und angefertigt bei

M. Sc. Nils Jakobs

Institut für Verbrennungstechnik

Deutsches Zentrum für Luft- und Raumfahrt



**FH AACHEN**  
UNIVERSITY OF APPLIED SCIENCES

# Declaration of Originality

Bachelor Thesis of Mohamed Anes Asmi (B. Eng. Aerospace Engineering)

Address Pfaffenwaldring 38-40, 70569 Stuttgart


Matriculation number 3234728

English title Development of a testing framework for evaluation of an aircraft engine controller

German title Entwicklung eines Testing-Frameworks zur Evaluierung eines Triebwerksreglers

I hereby declare

- that I have written this work independently,
- that no sources other than those cited have been used and that all the statements taken from other work, directly or figuratively, have been comprehensively listed,
- that the work submitted was not the subject of any other examination process, whether in its entirety or in substantial parts,
- that I had not published the work in whole or in part, and
- that during the elaboration of this work, all rights of intellectual property have been respected and that any external sources were used according to scientific writing norms.



.....

Aachen, 29.11.2023



## **Bachelorarbeit**

### **Entwicklung eines Testing-Frameworks zur Evaluierung eines Triebwerksreglers**

#### **Aufgabenstellung:**

Eine im Vergleich zum konventionellen Kreislauf modifizierte Gasturbine benötigt aufgrund der entsprechenden Anpassungen des Water-Enhanced-Turbofan-Antriebskonzeptes eine neue Regelungseinheit. Hierfür wird die ursprünglich verbaute pneumatisch-mechanische Regeleinheit durch eine elektronische Regelung ersetzt.

Im Rahmen der Bachelorarbeit wird ein bestehendes Matlab/Simulink Modell des Allison M250 Triebwerks inklusive Kraftstoffregler um ein Regler-Testing-Framework erweitert. Zu Beginn werden für die Regelung relevante Betriebs- und Anlagenparameter vom Studenten identifiziert und mit Hilfe des Testing-Frameworks untersucht. Das Framework variiert automatisiert verschiedene Betriebs- und Anlagenparameter und bewertet die erzielte Reglerstabilität. Daraufhin werden weitere für die Triebwerksregelung relevante Störgrößen qualitativ identifiziert und entsprechende Modellerweiterungen entwickelt, um in der zweiten Phase das Testing-Framework diesbezüglich zu erweitern.

#### **Arbeitspakete:**

- Einarbeitung in die Grundlagen (Modellierung, Test-Automatisierung, Regelung) (2 Wochen)
- Charakterisierung der Regelstrecke (1 Woche)
- Identifizierung der Regelparameter (2 Wochen)
- Erweiterung des Test-Frameworks und Ergänzung des Modells (2-3 Wochen)
- Auswertung und Dokumentation (1-2 Wochen)

#### **Ort und Dauer der Arbeit:**

Die Bachelorarbeit ist am DLR-Institut für Verbrennungstechnik durchzuführen und innerhalb von 9 Wochen nach offizieller Anmeldung abzuschließen.

#### **Betreuer:**

M.Sc. Nils Jakobs

# Abstract

This bachelor thesis presents a testing framework that has been developed for the evaluation of a model of a digital controller for the M250-C20B turboshaft engine. The thesis was conducted at the Institute of Combustion Technology of the German Aerospace Center in the context of the upgrade of the engine to a demonstrator of the Water Enhanced Turbofan.

The framework is a complete package written in MATLAB<sup>®</sup> code language that enables to vary parameters in a Simulink<sup>®</sup> simulation model of the engine. These parameters can be steady-state or transient and apply to the operation of engine above idle. The framework also enables to evaluate the system's controller response to the variations and apply numerical methods to optimize the simulation.

This work's findings contribute to the application of standardized numerical solutions for the development of digital controls for conventional Brayton-cycle-based gas turbines.

**Keywords:** controller testing, gas turbine, above-idle

# Acknowledgment

I would like to deeply thank my supervisor Prof. Dr.-Ing. Philipp Hartmann for his valuable guidance and feedback in his supervision of this thesis.

My profound gratitude goes to my co-supervisor Nils, who provided me with excellent insight into the subject and assisted me in the materialisation of this work.

I am also extremely grateful to all the members of the MGT department of the Institute of Combustion Technology at DLR, where I would especially like to thank the members of the System-Analysis team Dr.-Ing. Martin Henke and Mr. Thomas Krummrein for their technical remarks and reflections. I want also to thank Mr. Saeed Izadi for his ideas around the subject.

No one has been more supportive to me during my studies than the members of my family, to whom I would like to dedicate this work. I will always be indebted to my parents Faten and Abdesslem and my sister Ameni, who have always inspired me and paved the way for me to choose this course of studies. My thanks also go to my cousin Bassem, for his encouragement and devotion in all situations since my arrival in Germany.

All thanks to Allah.

# Table of contents

1.	Introduction .....	1
1.1	Presentation of the project.....	1
1.2	Allison M250-C20B .....	1
1.3	The M250 as a WET demonstrator .....	3
1.4	Objective of the thesis .....	4
2.	Theoretical principles .....	5
2.1	Introduction to control theory .....	5
2.2	Controller evaluation criteria .....	9
2.3	Evaluation architecture.....	12
2.4	Design of Experiment.....	14
3.	Structure of the simulation model .....	18
3.1	Turboshaft engine operation.....	18
3.2	Simulation model .....	20
4.	Implementation of testing framework .....	26
4.1	Structure of the framework.....	26
4.2	Identification of key system parameters.....	28
4.3	Parameter variation schemes .....	31
4.4	Implementation of evaluation criteria .....	33
4.5	Evaluation of sensitivity to disturbance .....	35
5.	Validation of results and discussion.....	36
5.1	Test case .....	36
5.2	Result of the full factorial design .....	38
5.3	Assessment of the response model.....	46
5.4	Augmentation of the response model with RSM .....	48

5.5	Analysis of the disturbance effect of power demand .....	50
6.	Summary .....	52
7.	References .....	53
	List of figures .....	56



# List of Symbols

<i>Latin Symbols</i>		
Symbol	Unit	Description
$A, B$	-	affine transformation coefficients
$b$	rpm.s	regression coefficient
$e$	-	error function
$f$	-	function
$G$	-	transfer function
$I$	kgm <sup>2</sup>	moment of inertia
$i$	-	sum index
$k$	-	number of factors
$l$	-	number of levels
$K_d$	-	derivative factor
$K_i$	-	integral factor
$K_p$	-	proportional factor
$Md$	N	torque
$\dot{m}$	g/s	mass flow
$N$	rpm	rotational speed
$N1$	rpm	rotational speed of N1-shaft
$N2$	rpm	rotational speed of N2-shaft
$n$	-	cardinal number
$P$	W	power
$p$	Pa	pressure
$r$	-	input function/setpoint
$s$	-	Laplace complex variable
$T$	K/°C	temperature
$T_d$	s	delay time
$T_i$	s	integral time
$t$	s	time
$t_r$	s	rise time
$t_s$	s	settling time
$u$	-	controller output function
$x$	-	coded factor value
$Y$	rpm.s	mathematically calculated response
$\bar{Y}$	rpm.s	average calculated response
$y$	-	output function/process variable
$z$	-	disturbance function

<i><b>Greek Symbols</b></i>		
Symbol	Unit	Description
$\Delta P_{el}$	W	step input of power demand
$\mathcal{L}$	-	Laplace transform
$\eta$	-	isentropic efficiency
$\sigma$	-	real part
$\tau$	s	integration variable
$\omega$	rad. s <sup>-1</sup> , -	angular velocity, imaginary part

# List of Subscripts

0	initial
100%	design speed in percent
a	actual
amb	ambient
comb	combinations
comp	compressor
effect	effect
el	electrical
end	end
FADEC	relating to FADEC
fuel	relating to fuel
IAE	integral absolute error
IE	integral error
init	initial
ISE	integral squared error
ISAE	integral time squared error
ITAE	integral time absolute error
LPT	relating to low pressure turbine
max	maximal
MGU	relating to motor generator unit
min	minimal
N1	relating to high pressure shaft
N2	relating to low pressure shaft
red	reduced
s	isentropic
s,m	isentropic from map
step	step
turb	turbine

# List of Abbreviations

<b>CCD</b>	central composite design
<b>CCF</b>	central composite face-centred
<b>DLR</b>	German Aerospace Center
<b>DoE</b>	Design of Experiment
<b>EEC</b>	electronic engine control
<b>FADEC</b>	full authority digital engine control
<b>FCS</b>	fuel control system
<b>GPFC</b>	gas producer fuel control
<b>GTE</b>	gas turbine engine
<b>HIL</b>	Hardware-in-the-Loop
<b>HP</b>	high pressure
<b>HPT</b>	high pressure turbine
<b>IAE</b>	integral absolute error
<b>IE</b>	integral error
<b>ISE</b>	integral squared error
<b>ISAE</b>	integral time squared error
<b>ITAE</b>	integral time absolute error
<b>LP</b>	low pressure
<b>LPT</b>	low pressure turbine
<b>M250</b>	Allison M250-C20B
<b>MCU</b>	motor control unit
<b>MGU</b>	motor generator unit
<b>MGTS<sup>3</sup></b>	Micro Gas Turbine Steady State Simulator
<b>NO<sub>x</sub></b>	nitrogen oxide
<b>ODE</b>	ordinary differential equation
<b>PI</b>	proportional-integral
<b>PID</b>	proportional-integral-derivative
<b>PTG</b>	power turbine governor
<b>PV</b>	process variable
<b>RSM</b>	response surface methodology
<b>SISO</b>	single-input single-output
<b>SP</b>	setpoint
<b>TIT</b>	turbine inlet temperature
<b>WET</b>	water enhanced turbofan

# 1. Introduction

## 1.1 Presentation of the project

The project *LuFo DinA2030+* of the Institute of Combustion Technology of the German Aerospace Center (DLR) aims at the development of a demonstrator for the Water Enhanced Turbofan (WET) technology. It is supported by the German Ministry of Economy and Climate Protection along with a third-party manufacturer of aircraft propulsion systems. The WET technology is a promising concept that would enable, through the injection of vaporized water in the combustor, to reduce the amount of harmful combustion emissions as well as improve engine efficiency [1]. The proposed demonstrator is based on a modified Allison (rebranded Rolls-Royce) M250-C20B turboshaft gas turbine.

The planned integration of the WET technology in the gas turbine necessitates an upgrade of the conventional turbine systems, which are customized in their design to the flight mission of helicopters. For this reason, an upgrade of the engine control system into a digital controller is also put forth, which would enable more versatility for the integration of the technology [1].

Moreover, it has also been planned to test the new controller using a Hardware-in-the-loop (HIL) simulation, where its physical dynamics can be investigated under real conditions within a simulation incorporating a model of the engine that has been developed for the purpose.

However, a testing and evaluation methodology for the controller needs to be drafted by first incorporating it into the digital engine model and studying its dynamics even before the HIL stage can be initiated. Essentially, this step should validate the controller against any model-related inaccuracies compared to the real system. Furthermore, for an aspired easy incorporation of the WET components, any misjudgement of cycle parameters should be anticipated in the design of the controller. The goal of this thesis is to develop a testing framework for the purpose of achieving a complete assessment of the controller by modifying cycle parameters and qualifying disturbance parameters.

## 1.2 Allison M250-C20B

The turboshaft engine Allison M250-C20B, targeted by the WET upgrade in the scope of the project *LuFo DinA2030+*, is a model of the Allison M250 engine family that counts more than

# 1 Introduction

31 000 produced units found in a variety of uses in aviation and automotive sectors. However, its main application remains as that of a helicopter powerplant thanks to its compact design and numerous features, e.g., its reverse flow combustor and its constant speed configuration . [2]

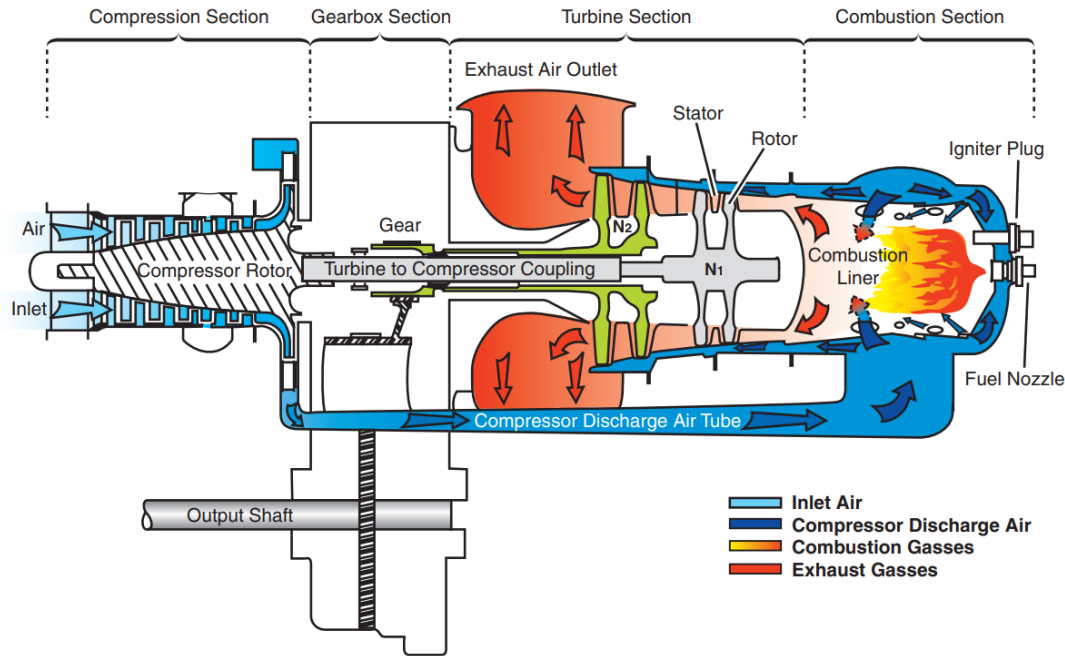


**Fig. 1. Cross-section view of the M250-C20B [3]**

Illustrated in Fig. 1 are the internal components of the M250-C20B (later referred to as only M250) and its twin-shaft design. The first shaft is the gas producer shaft, referred to as N1-shaft, transmitting power between a seven-stage compressor and a two-stage high-pressure turbine. The second shaft is the power shaft, also referred to as N2-shaft, transmitting power from a two-stage low-pressure turbine to the output shaft via a gearbox.

**Table 1.1. M250-C20B engine ratings at sea level [4]**

	Est. Shaft Power /kW	N1 /rpm	N1 /%	N2 /rpm	N2 /%
Flight Idle	26	36 114	71	33 290	100
75 % Maximum Cruise	207	46 860	92	33 290	100
90 % Maximum Cruise	248	48 120	94	33 290	100
100 % Maximum Cruise	276	51 180	100	33 290	100
Maximum Take-off	313	53 000	104	33 290	100

## 1 Introduction

The rotational speed  $N_1$  of the N1-shaft varies from around 36 000 rpm at idle to 50 970 rpm at 100% cruise speed (at sea level) while the N2-shaft rotates at a speed  $N_2$  of 33 290 rpm at 100% cruise speed (also at sea level). The M250 has a maximum cruise power rating of 276 kW with a maximum take-off power of 313 kW (refer to Table 1.1).

### 1.3 The M250 as a WET demonstrator

To demonstrate the integration of WET technology in an aero engine, the M250 was commissioned as ground test rig installed in the DLR laboratory, which is intended to be refitted with WET components.

Historically, the WET technology was first introduced as an approach to decrease emissions in aviation by targeting the combustion process such that nitrogen oxide ( $\text{NO}_x$ ) emissions and other combustion-related effects are reduced. In addition, it aims at improving the efficiency of the thermodynamical cycle by increasing the gas mass flow entering the turbine and thus increasing the specific power of the engine system. This is done by injecting water vapor during the combustion phase and regaining it via condensation from the exhaust gases. [1]

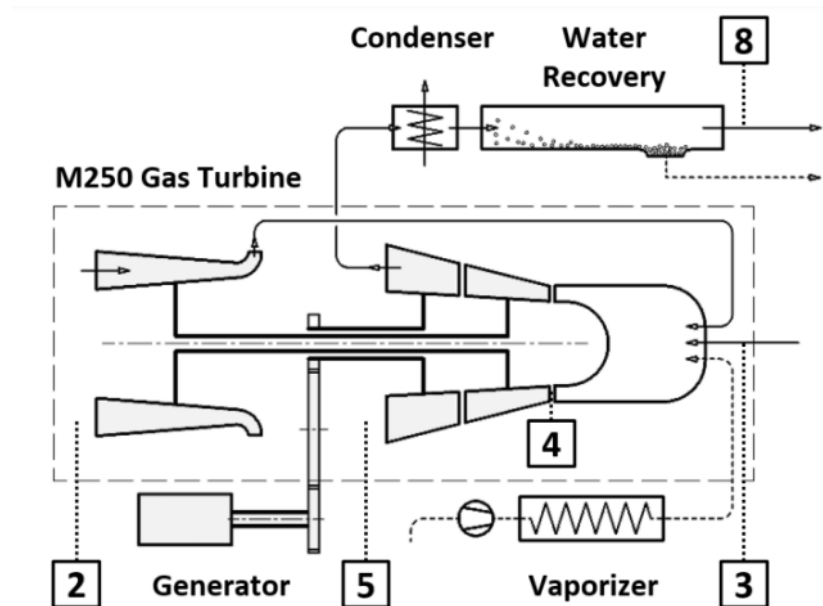


**Fig. 2. Integration of WET components into the M250 engine [1]**

The intended upgrades on the M250 exhibited in Fig. 2 include the fitting of a water evaporation line, which incorporates a vaporizer, water vapor injector, and a water recovery unit along with a condenser [1]. The relatively simple upgrades and the reduced of number of additional

## 1 Introduction

components allows for the WET technology to be applied to almost any engine applying the Brayton cycle, although the technology itself is named in reference to turbofan engines, being its main target and the major engine type powering commercial aircrafts.

The simplicity of the original M250 design allows, via a conventional pneumatic-hydraulic fuel controller, to adapt the fuel flow proportionally to the power demand. However, in contrast to the normal “dry” combustion process, the WET technology requires recalibrating the air-to-fuel ratio and thus changing the amount of injected fuel. To properly investigate new combustion conditions imposed by the WET cycle, the original fuel controller needs to be replaced by an electronic engine controller [1].

Considering these limitations and requirements, an early version of a Full Authority Digital Engine Control (FADEC) that incorporates an Electronic Engine Controller (EEC) for the M250 has been designed. The FADEC is intended to replace the original Fuel Control System (FCS) and should enable the operation of the gas turbine outside the mission envelope it was originally designed for, such as in the case of the operation as WET demonstrator. However, this early version of the FADEC must be first proved with the original M250 before any cycle modifications can be introduced.

### 1.4 Objective of the thesis

A simulation model that is based on technical and physical properties of the forementioned engine has been developed for the study of the upgrades that will accompany the integration of WET technology. The purpose of this work is to develop a testing framework for the simulation model that would enable to evaluate the performance of the early version of the FADEC when different system parameters are varied, including cycle parameters. Moreover, the framework should enable to diagnose the effects resulting from disturbance parameters.

The performance within the scope of this work will be only investigated for the operation of the engine post Flight Idle, whereas performance assessment during the engine’s start and below Flight Idle will be investigated in parallel by a different party within the project. Moreover, as the M250 is currently installed as a laboratory test rig, only controlled ambient conditions for the operation will be accounted for in this work.



## 2. Theoretical principles

In this chapter, the theoretical principles used in this work will be presented and explained, while highlighting the reasons behind their implementation in the system and the framework.

### 2.1 Introduction to control theory

The control engineering is the branch of engineering devoted to process control and automation. In any operating plant, the control loop is critical to guarantee satisfactory results of the process and compensate for equipment degradation or even cases of faulty hardware. While a manual calibration of the control loop to the plant characteristics is possible, in the context of digital control, it is more favourable to automate the monitoring of the performance of the control loop. [5]

#### 2.1.1 General control loop

The control system treated in this work is a single-input-single-output (SISO) closed-loop system. Fig. 3 shows a closed control loop where the measured signal  $y(t)$  (also called process variable PV) is fed back to the input/reference signal  $r(t)$  (also called setpoint SP), to determine the control error  $e(t) = r(t) - y(t)$ . In this simple control-loop made up by a controller block and a plant block, the purpose of the controller is then to keep the control error at a minimum while also compensating for the disturbance signal  $z(t)$  affecting the plant's behaviour. [6]

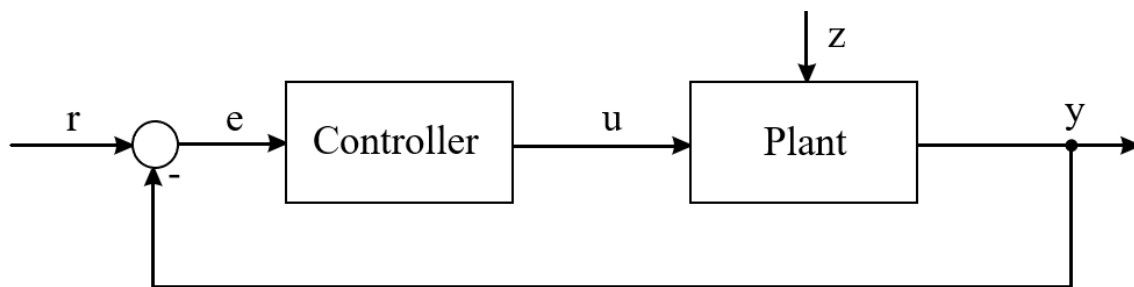


**Fig. 3. Feedback control loop**

#### Transformation from time domain to frequency domain

In theoretical control systems, to investigate the relationship between the input and the output signal in a control loop, a transfer function  $G$  is defined using the dynamics of the system such as physical laws or the definition of the system itself.

## 2 Theoretical principles

Before such a function can be deduced, usually a transformation from the time domain to the frequency domain is performed. This is done with the help of the Laplace transform  $\mathcal{L}$ , an integral transform function employed to simplify the expression of a function  $f$  by transforming the time variable  $t$  to a complex frequency variable  $s = \sigma + i\omega$  and defining a new function  $F$  of  $s$  [6].

$$f(t) \xrightarrow{\mathcal{L}} F(s)$$

By applying the Laplace transform to the input and output functions  $r(t)$  and  $y(t)$  schematised in Fig. 3, the input and output functions in the frequency domain  $R(s)$  and  $Y(s)$  are obtained. The transfer function of the block is then defined as  $G(s) = \frac{Y(s)}{R(s)}$  [7].

For example, in this closed control loop made up only of a controller and a plant with the respective transfer functions  $G_c$  and  $G_p$ , the closed loop's transfer function  $G$  is defined in function of the transfer functions of the two blocks as [6]

$$G(s) = \frac{Y(s)}{R(s)} = \frac{G_c}{1 + G_c \cdot G_p}. \quad \text{Eq. 2.1}$$

When the concept of the closed control loop is applied to the combination of the M250 and the envisioned FADEC, it results in a comparable closed control loop to that detailed in Fig. 4. While the grey-boxed FADEC represents the entire controller package, only the controller block inside it representing the EEC will be simulatively assessed, as the actuators and sensors are the hardware interface to the engine for signal conversion and feedback and will be evaluated within a HIL test setup.

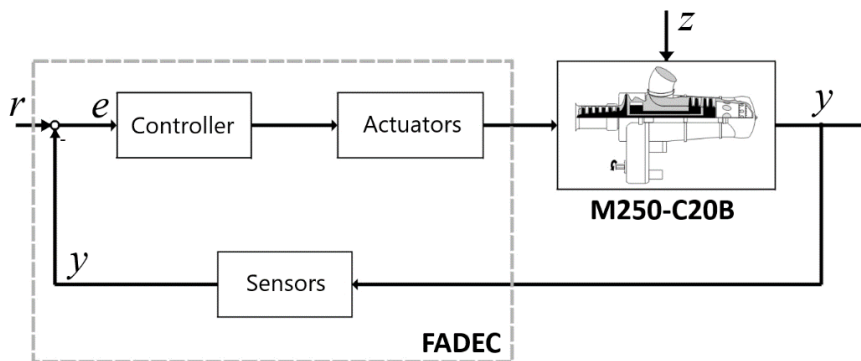


**Fig. 4. The conventional control loop applied to the M250-C20B [8]**

## 2 Theoretical principles

Moreover, by applying the concept of Laplace transform and Eq. 2.1 to the loop in Fig. 4 where  $G_{\text{FADEC}}$  and  $G_{\text{M250}}$  are the respective transfer functions of the FADEC and of the M250, the following closed loop transfer function is obtained

$$G(s) = \frac{Y(s)}{R(s)} = \frac{G_{\text{FADEC}}}{1 + G_{\text{FADEC}} \cdot G_{\text{M250}}} . \quad \text{Eq. 2.2}$$

However, for real systems, the plant usually does not have proper a transfer function that can be used to investigate the system behaviour. As it will be further discussed later, the M250 represents a non-linear system with no explicit transfer function  $G_{\text{M250}}$ . Hence the system response will be assessed for different setpoints using non-analytical evaluation methods.

### 2.1.2 PID controller

The controller illustrated in Fig. 5 is a proportional-integral-derivative (PID) controller in its parallel form. Used broadly in the industry thanks to its simple control strategy, it is made up by three main components: a proportional block with the control function  $u_p(t) = K_p \cdot e(t)$ , an integral block with the function  $u_i(t) = K_i \int_0^t e(\tau) d\tau$  and a derivative block with the function  $u_d(t) = K_d \cdot \frac{d}{dt} e(t)$ .

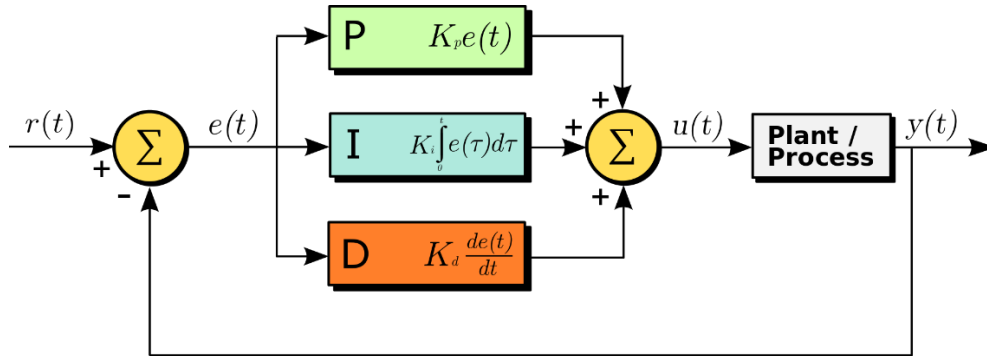


**Fig. 5. PID controller structure [9]**

When given an error signal  $e(t)$  as an input, the controller outputs the signal  $u(t)$  with the following expression in the time domain [6]

$$u(t) = K_p \cdot e(t) + K_i \int_0^t e(\tau) d\tau + K_d \cdot \frac{d}{dt} e(t) . \quad \text{Eq. 2.3}$$

## 2 Theoretical principles

This overall function shows how each mathematical term reacts to the error signal; the proportional summation term represents the current error, while the integral summation compensates for the past error after the integral time  $T_i$  and the derivative summation term tries to predict the error after a certain future delay time  $T_d$ .  $T_i$  and  $T_d$  are respectively defined as the integral time and the delay time constants.

The parallel form of PID controller is not suitable for tuning, as the factors  $K_p$ ,  $K_i$  and  $K_d$  do not show any physical or mathematical connection. A more general form is then introduced by factorizing  $K_p$ . The following expression is then obtained [6]

$$u(t) = K_p \cdot \left( e(t) + \frac{K_i}{K_p} \cdot \int_0^t e(\tau) d\tau + \frac{K_d}{K_p} \cdot \frac{d}{dt} e(t) \right). \quad \text{Eq. 2.4}$$

Replacing  $\frac{K_i}{K_p}$  with  $\frac{1}{T_i}$  and  $\frac{K_d}{K_p}$  with  $T_d$  results in the following ideal transfer function

$$u(t) = K_p \cdot \left( e(t) + \frac{1}{T_i} \cdot \int_0^t e(\tau) d\tau + T_d \cdot \frac{d}{dt} e(t) \right). \quad \text{Eq. 2.5}$$

An example of a step response of the PID-controller is depicted in Fig. 6, where the output signal is composed by the components of the transfer function. The proportional term (P-term) controls the signal's gain at  $t = 0$ , while the integral term (I-term) gives the ramp of the signal in function of the time. Due to derivative term (D-term), a Dirac delta function is observed for the signal at  $t = 0$  [6].

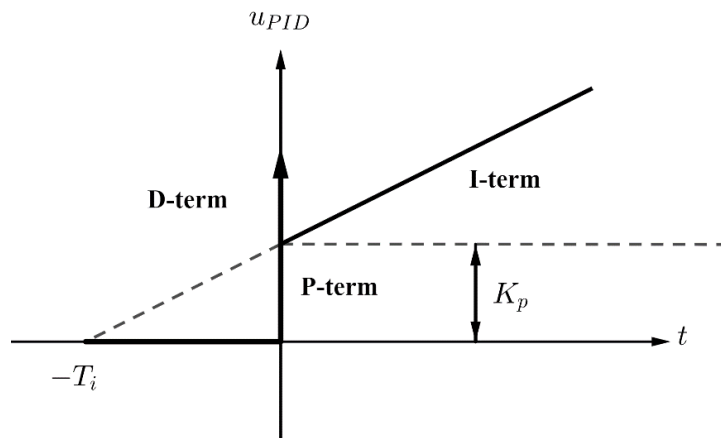


**Fig. 6. Step response of a PID controller (translated) [6]**

## 2 Theoretical principles

In return, to get the transfer function the PID controller from time-domain to frequency domain, Laplace transform is applied to the ideal form of the PID controller in Eq. 2.5

$$G(s) = K_p \cdot \left( 1 + \frac{1}{T_i \cdot s} + T_d \cdot s \right). \quad \text{Eq. 2.6}$$

This form is more commonly used as it allows to establish a physical interpretation of the coefficients from the controller response and thus tune it more easily using empirical methods [10].

### 2.1.3 PI controller

The PI controller is a simplified version of the PID controller where the derivative component is not included in the summation. Although the derivative component increases the reactivity to control errors [6], the PI-controller offers the advantage of being more tolerant to feedback signal errors caused by signal noise or transport delay by eliminating the predictive behaviour of the signal derivation, thus rendering it more adequate to industrial applications [10].

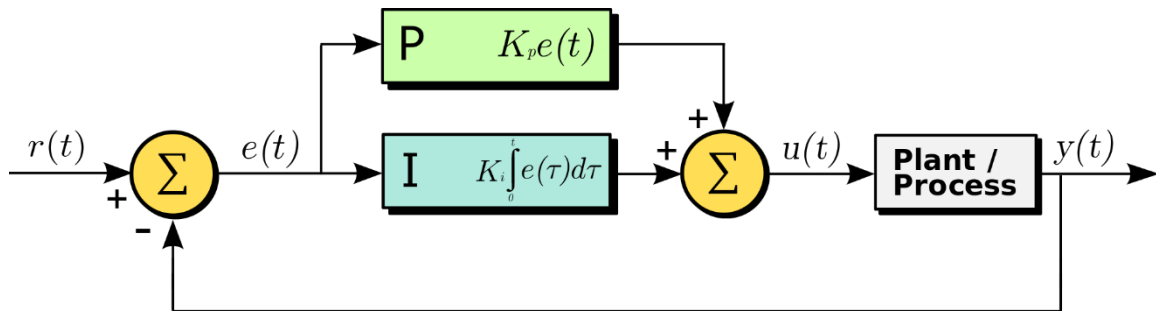


**Fig. 7. PI controller structure [9]**

During this work, the EEC inside the FADEC is built as a PI-controller with the following transfer function

$$G(s) = 1 \cdot \left( 1 + \frac{1}{3s \cdot s} \right). \quad \text{Eq. 2.7}$$

## 2.2 Controller evaluation criteria

The controller's purpose is keeping the signal error between the measured and the reference signal at a minimum. Throughout this work, the evolution of the error with the simulation time

## 2 Theoretical principles

will be exploited to evaluate the performance of the controller. Based on pre-characterised setpoints fed into the simulation, a variation is used to trigger a respective system response and assess it. In this context, two main evaluation methods will be used: time-domain characteristics and response curve criteria.

### 2.2.1 Time-domain characteristics

The time-domain characteristics analyse the dynamics of the response signal. In Fig. 8, some of the traditionally-used characteristics in industry are presented, that are also applicable to any system and allow to get a first idea of its dynamic behaviour [5].

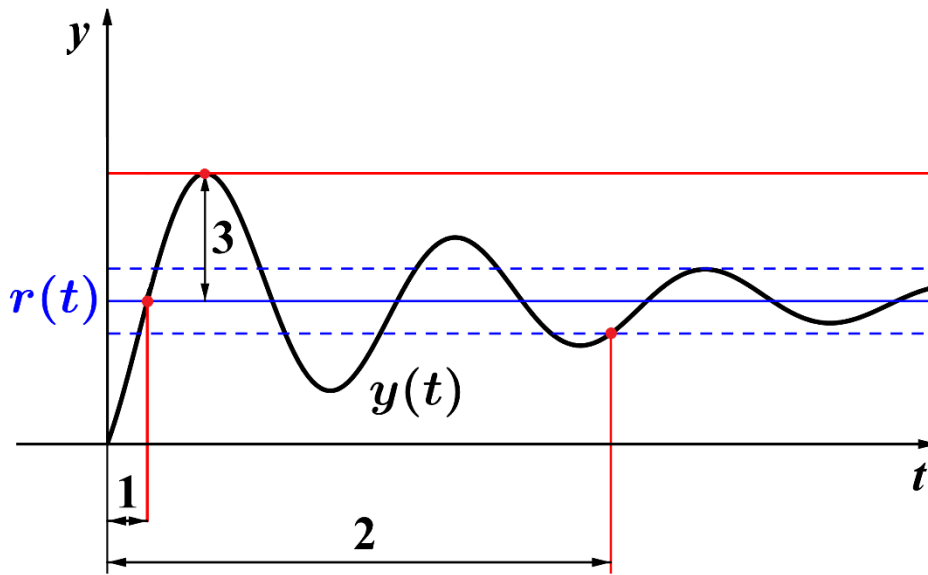


**Fig. 8. Response time-domain criteria. 1:  $t_r$ , 2:  $t_s$ , 3: OS**

**1- Rise time  $t_r$ :** the time needed for the measured response  $y(t)$  to reach a determined percentage of the change in the reference value  $r(t)$ .

**2- Settling time  $t_s$ :** the time needed for the measured response  $y(t)$  to settle inside a definite band of the reference value  $r(t)$ .

**3- Overshoot OS:** the maximum excess error reached expressed as a percentage of the change in the reference value  $r(t)$ .

## 2 Theoretical principles

### 2.2.2 Response curve criteria

Alternatively, the response curve criteria, also known as integral error measures, are used as an index to compare the response globally and emphasize any long lasting errors from the response such as continuous oscillations [11].

In a transient change of the setpoint for the signal, a cumulative scalar value  $Y_{IE}$  of the signal error  $e(t)$  over the entire simulation range can be determined using the integral error (IE).

Each of the following methods has its own advantages owing to the mathematical nature of the expression and suits a specific response behaviour better than others. [12]

#### **Integral Square Error**

The Integral Square Error (ISE) method (see Fig. 9-a) allows to magnify the large errors during the transition of the signal to the new setpoint. This is used when larger errors can penalize the performance of the system and need to be avoided [12].

$$Y_{ISE} = \int_0^{\infty} e^2(t) dt \quad \text{Eq. 2.8}$$

#### **Integral Absolute Error**

The Integral Absolute Error (IAE) method (see Fig. 9-b) gives a total value of the error by calculating the sum of the areas above and below the signal separating it from its reference [5].

$$Y_{IAE} = \int_0^{\infty} |e(t)| dt \quad \text{Eq. 2.9}$$

#### **Integral Time Squared Error**

In analogy to the ISE method, the Integral Time Squared Error (ITSE) magnifies the larger errors in the signal (see Fig. 9-c), but also penalizes later signal fluctuations. Thus, it is a measure of responsiveness quality of the system [13].

$$Y_{ITSE} = \int_0^{\infty} t \cdot e^2(t) dt \quad \text{Eq. 2.10}$$

### Integral Time Absolute Error

Like the IAE method, the Integral Time Absolute Error (ITAE) (see Fig. 9-d) not only takes into account the error from the reference signal in both directions without accentuating its order, but also scales the longer lasting errors in the final value [12].

$$Y_{ITAE} = \int_0^{\infty} t \cdot |e(t)| dt \quad \text{Eq. 2.11}$$

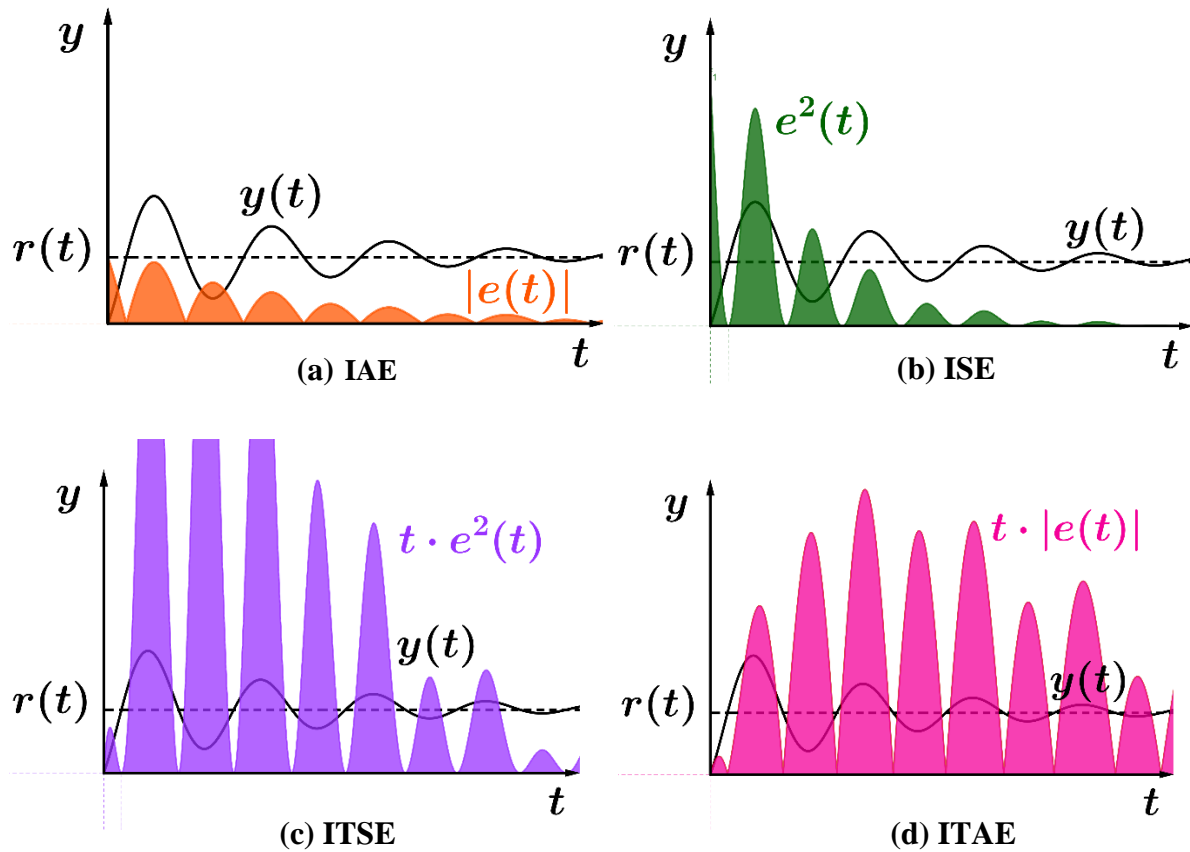


Fig. 9. Graphical illustration of response curve criteria

### 2.3 Evaluation architecture

Since the considered approach during this work is purely simulative and is based on variation of parameters, it is essential to apply an adequate methodology in the preparation of the simulation. This also means minimizing the number of simulations runs needed and the required computational power, thanks to an efficient selection of the parameter ranges based on their effects. [14]



## 2 Theoretical principles

For this matter, an approach based on Design of Experiment (DoE) was followed. DoE generally describes the methodology to reduce the time of experimental trials by investigating experimental (or simulative) responses of a limited number of cases and producing an efficient design sheet based on the number of factors (variable parameters) and the levels for each factor (the value assigned to the parameter at each run) [15].

In the work of *Alvarez et al.* [16], a statistical methodology was developed to analyse the sensitivity of computer aided Very Large Scale Integration-device. This work was considered during the conception of the framework as it handles the optimization of processes characterized by a large number of parameters (more than 5). Based on this reference, the architecture of the framework is divided into four waypoints: synthesis, analysis, optimization, and design for manufacturability.

### **Synthesis**

The synthesis englobes the creation and parameterization of the simulation model [16]. As part of this work, this step includes the preprocessing of the test cases of a parametric study that will be further discussed later.

### **Analysis**

The analysis is primarily a step during which an initial definition of input parameters as well as output responses is required. Accordingly, a valid operation range is then defined, based on which a screening test is carried out to identify the key factors for the responses.

In a second phase response surface methodology (RSM) is applied to design a testing matrix that covers the operation range of the most important factors. The application of the RSM designs and their different characteristics and results will be discussed later. [16]

### **Optimization**

During the optimization phase, the input parameters are classified as being global or specific. Global parameters are presented as affecting a wide range of responses, while specific parameters are only localised to a few responses. [16]

### **Design for Manufacturability**

## 2 Theoretical principles

This waypoint is intended to minimize the sensitivity of the critical responses to global factors using the advantage of specific input factors. Usually, the global parameters in question present a certain difficulty to control, e.g., an increase in power demand due to wind effects on the rotor connected to the M250. However, in the context of this work, this phase is little applicable due to the aim of investigating critical responses. Instead, this will be introduced as an extension of the model for handling disturbance effects after the implementation of the three first foundations of the framework.

### 2.4 Design of Experiment

The DoE regroups all the techniques used in planning experiments to deduct conclusive results. Based on the objective of the experiment, or simulation in this context, various design approaches are taken. In this work, screening and RSM designs will be discussed. In general, a screening design is exploited to identify the important effects of the parameters, while an RSM design uses the vertices of the input vector to limit the number of experimental runs required. [15]

#### 2.4.1 Screening design

The screening design is either a full or a fractional factorial design where all varied parameters are given two levels: a maximal and a minimal value. The factorial points, also defined as geometrical vertices of the factorial space, coloured red in Fig. 10, usually correspond to the validity range of the parameter, e.g., a physical definition.

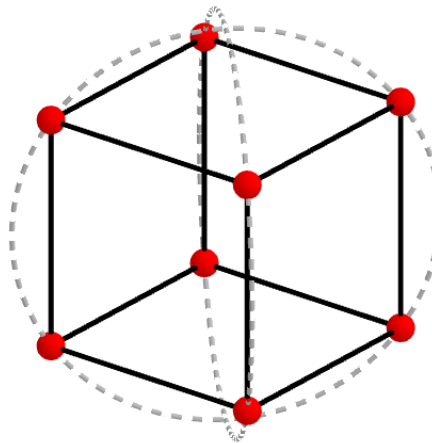


**Fig. 10. Illustration of full factorial design for three factors**

## 2 Theoretical principles

A full factorial screening design can be time demanding as the number of combinations the resulting simulation runs needed is doubled with each additional factor, with the number of combinations  $n_{\text{comb}}$  for  $k$  factors with  $l$  levels obeying the following rule

$$n_{\text{comb}} = l^k. \quad \text{Eq. 2.12}$$

### 2.4.2 Response surface methodology

In addition to vertices, centre points can be employed to assess the presence of a quadratic variation of the response. However, this can significantly increase the required amount of runs as another level is added, and thus needs to be applied carefully using some proven methods. This is the case with RSM designs, where a selected number of factorial point runs are combined with centre points runs known as “control runs”.

Two main design models are used as part of RSM: *Box-Behnken* and central composite design (CCD). CCD is itself divided into three subcategories, where in the scope of this work, only the subcategory central composite face centred (CCF) will be applied as model.

#### **CCF model**

Shown in Fig. 11-a is a model of a three-factor CCF design. The model regroups factorial points or vertices (dark blue) along with axial points representing the centre of each design surface or plane (cyan), and a centre point in the middle of the design (medium blue). [16]

#### ***Box-Behnken* model**

The second type of quadratic design illustrated in Fig. 11-b, *Box-Behnken*, uses the midpoints of the edges of the process space (light green) in addition to a centre point run (dark green). In contrast to CCF, *Box-Behnken* designs contain regions of poor prediction due to the lack of vertices. Moreover, they combine centre points and edge points in one run, which means that the variation from a full factorial run cannot be included. [15]

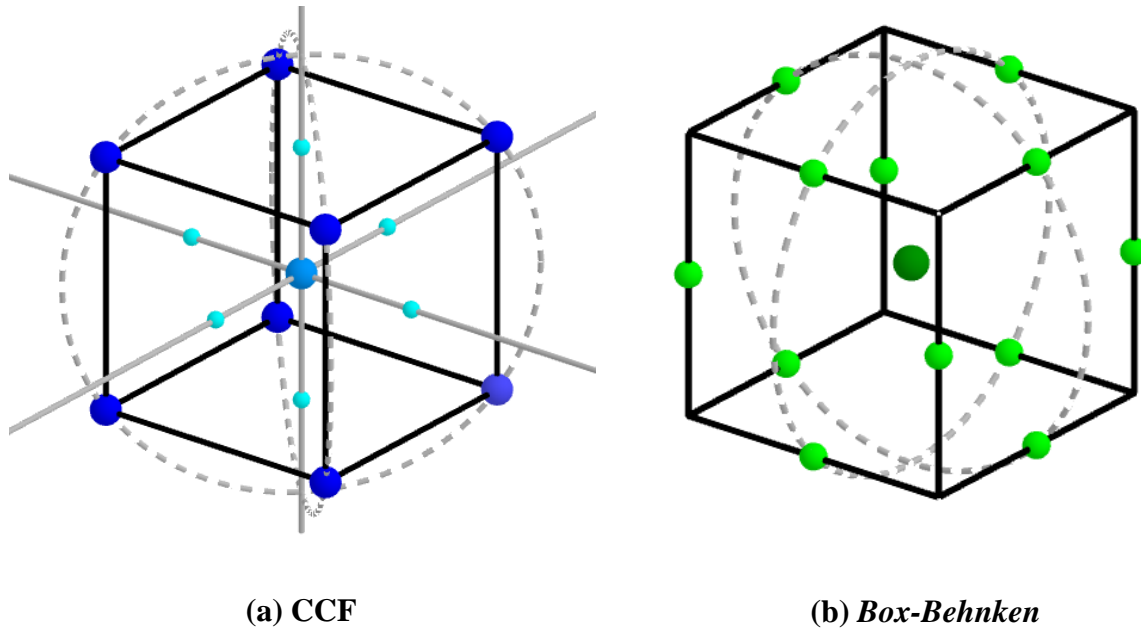


**Fig. 11. Illustration of RSM designs for three factors**

Table 2.1 shows an example of a design sheet using CCF and *Box-Behnken* models compared with a full factorial screening design. For less than three factors, a *Box-Behnken* design requires fewer runs in comparison to CCF, whereas for more than four factors, this advantage is cancelled.

**Table 2.1 Comparison of full factorial, CCF and a *Box-Behnken* design for three factors [15]**

Full Factorial			Box-Behnken			CCF		
$X_1$	$X_2$	$X_3$	$X_1$	$X_2$	$X_3$	$X_1$	$X_2$	$X_3$
-1	-1	-1	-1	-1	0	-1	-1	-1
1	-1	-1	1	-1	0	1	-1	-1
-1	1	-1	-1	1	0	-1	1	-1
1	1	-1	1	1	0	1	1	-1
-1	-1	1	-1	0	-1	-1	-1	1
1	-1	1	1	0	-1	1	-1	1
-1	1	1	-1	0	1	-1	1	1
1	1	1	1	0	1	1	1	1
			0	-1	-1	-1	0	0
			0	1	-1	1	0	0
			0	-1	1	0	-1	0
			0	1	1	0	1	0
			0	0	0	0	0	-1
						0	0	1
						0	0	0

## 2 Theoretical principles

The numbers in the table represent the coded values for each factor, where the maximum and minimum values are respectively coded in -1 and 1, while 0 represents the midrange value. The scaling of values allows to compare the factors without having to refer back to their physical significance [15].

RSM has been applied intensively in industrial processes. However, due to the lack of experimental errors, its application in simulation models differs from the experimental-based notions [16]. On one hand, a model lack-of fit is the sole cause of difference between fitted and simulative results. In experimental designs, numerous centre point runs are usually conducted to compensate for the unaccounted real effects. In simulation, only one centre point is required to evaluate the model fit. On the other hand, all logistical and physical restrictions of an experimental design are annulled, such as rapid turnaround of experiment, simultaneous testing of multiple factors or randomizing of factors.

### 3. Structure of the simulation model

For the purpose of investigating the M250 engine and prepare for HIL experiments to test any planned upgrades in real time environment, a digital model of the entire engine had already been developed and implemented within a simulation tool. This model also includes the early version of the FADEC and the EEC that will be evaluated as part of this work.

To illustrate its implementation as a numerical simulation package, the background of operation and control of the original turboshaft engine is first presented, after which the simulation model is introduced.

#### 3.1 Turboshaft engine operation

The turboshaft is a type of gas turbine engine (GTE) that follows the Brayton thermodynamical cycle. Specifically, its purpose is the conversion of the chemical energy stored in the fuel mainly into a mechanical rotation, with an insignificant amount of thrust force resulting from the residual flow velocities at the exhaust. It incorporates two shafts, a high-pressure (HP) shaft for the main cycle and a low-pressure (LP) shaft delivering useful torque. The HP shaft is fitted with a compressor that is driven by a high-pressure turbine (HPT), while the LP shaft is fitted with a low-pressure turbine (LPT) that drives the load element [17]. In the M250, the HP shaft is the N1-shaft, while the N2-shaft represents the LP shaft.

In general, the turboshaft engine features a free turbine configuration (see Fig. 1), where the shafts are uncoupled from each other and are only aerodynamically dependent. This also means that the turbine on each shaft, i.e., the core engine shaft and the output shaft can rotate at different speeds. [17]

When mounted in a helicopter, the GTE powers the main rotor at a constant speed. This is to guarantee the aerodynamical efficiency of the rotor at all operation states and that no supersonic phenomena occur at the rotor blade tips [17]. While the rotor is designed for steady speeds, the amount of the lift generated can be varied using the collective blade pitch control in the cockpit. The collective pitch control, or collective lever, is one of the four main helicopter flight controls. It collectively varies the angle of attack of the rotor blades, adding or reducing torque demand from the main rotor shaft, which is compensated by the engine by increasing or decreasing power to the main output shaft, holding the shaft speed constant [4].

### 3 Structure of the simulation model

In the case of the M250 mounted in the laboratory of the Institute of Combustion Technology, the output shaft of the gas turbine is linked to a motor control unit-motor generator unit (MCU/MGU). In its MGU mode, the unit replaces the rotor of the helicopter and receives mechanical power from the engine to convert it into electrical current that is later transferred to a last bank [18]. The power demand of the MGU can be directly controlled by the operator and thus also the torque demand from the gas turbine, acting in the same manner to that of a collective lever in a helicopter.

#### 3.1.1 Original control system of the M250

In the M250, the N1-shaft and the N2-shaft are coupled to a gearbox that drives the engine accessories. These include on one side the starter, the fuel pump, and the gas producer fuel control (GPFC) that are driven by the N1-shaft, and on the other side the power turbine governor (PTG), that is connected to the N2-shaft.

Due to the earlier design of the M250, the control of the engine is mainly based on the fuel flow. The GPFC and the PTG make up the essential part of the engine fuel control in the M250 and follow a pneumatic-hydraulic system of valves and springs to dose the fuel flow to the combustor. Both are also fitted with levers that receive control input from the helicopter cockpit: the N1-lever and the N2-lever, linked to GPFC to PTG respectively. The remaining part of engine control consists in the compressor air-bleed valve, that assures compressor stability at different speed ranges, but cannot be operator-controlled. [4]

#### 3.1.2 Operation control of the M250

The control of the M250 is accomplished mainly via the N1-lever and N2-lever. The combination of the two levers divides the operation range of the M250 during a normal mission into three parts: from engine standstill, the start and ramp-up until the first idle speed is reached, known as Ground Idle. Then, through the input from the N1-lever, the transition from Ground Idle to a second idle level is achieved. After this second level, known as Flight Idle, the full power output of the engine becomes available and the engine control is then solely fulfilled by the N2-lever during the entire airborne operation until engine shutoff [4].

The three phases are distributed following the rotational speed of the engine shafts [4]:

### 3 Structure of the simulation model

**Before Ground Idle:** start of the engine and ramp-up transient phase where the control input is targeted at the stability of the core engine shaft and its N1 speed. (N2 is at around 75% of its cruise rating speed).

**Ground Idle to Flight Idle:** short transient phase where the control target is switched to the N2-shaft and the N2 speed moves from 75% to 100%.

**Post Flight Idle:** this covers the whole operation range of the engine when the helicopter is in flight, including take-off and landing stages. The N2 is kept at 100% of the throttle input, while the N1 compensates for torque variations.

## 3.2 Simulation model

The simulation model of the M250 is based on the Micro Gas Turbine Steady State Simulator (MGTS<sup>3</sup>) simulation tool, which was designed inhouse within the micro gas turbines department of the Institute of Combustion Technology of DLR in Stuttgart. The solver of simulation package that will be presented afterwards in this work is entirely based on it. It is highly modular and allows for an interconnection of the internal component models. The base simulation library has been extended to incorporate the model of the Allison M250 engine as an entire standalone package written in MATLAB<sup>®</sup> code and using Simulink<sup>®</sup> as a graphical user interface. It is worth noting that the implementation of the engine's model in Simulink<sup>®</sup> was only designed for fixed initial input parameters, although Simulink<sup>®</sup> usually allows parameter simulations with variable input. [19]

While the Simulink<sup>®</sup> model of the M250 is the core of the package used in this work, the external functions for communicating with it are inherited from MGTS<sup>3</sup>.

### Simulink<sup>®</sup> model

The Simulink<sup>®</sup> model (see Fig. 12) is made up using the conventional closed loop block diagram discussed in Paragraph 2.1. In addition to the controller-block containing the control algorithm and the plant-block containing the engine thermodynamical cycle and component maps, a feedback-block has been added that computes the rotation dynamics of the system. An additional block representing the inherited solver-block from the MGTS<sup>3</sup> package is connected to the system block and contains the simulation solver settings, but it will not be



### 3 Structure of the simulation model

further discussed during this work. Moreover, the arrows in Fig. 12 represent the flow of data between the blocks as implemented in Simulink®.

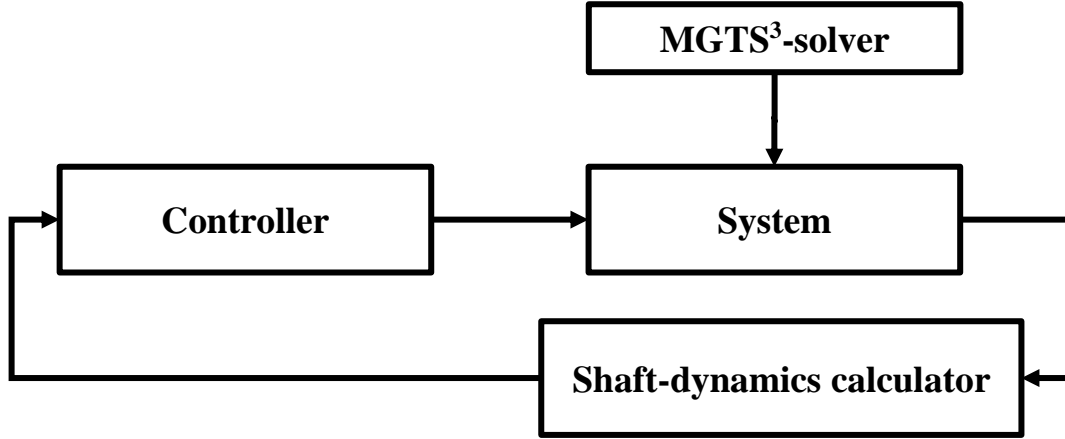


**Fig. 12 Structure of the Simulink® model used in the simulation.**

#### 3.2.1 Controller block

The controller block implemented in the Simulink® Model represents the EEC of the FADEC. While the sensors of the FADEC collect the feedback from the engine as engine parameters, it is the EEC that acts directly on the system based on these parameters. Similarly, the controller block acts on determined parameters that affect the behaviour of the system.

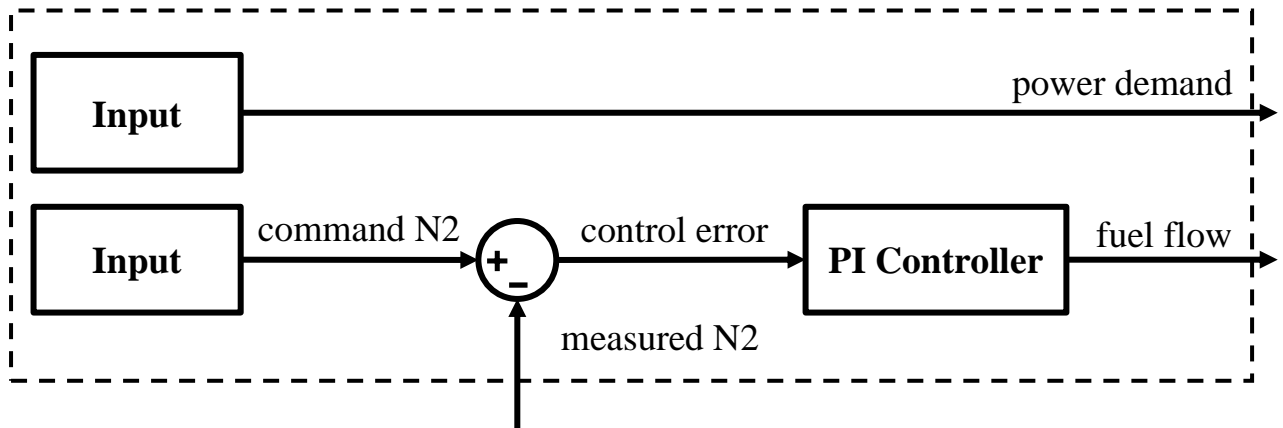


**Fig. 13. Model Controller Block**

The internal structure of the controller is revealed in Fig. 13, which is made up of a PI controller and a power demand block for the power output to the MGU. The PI controller directly affects the fuel mass flow to the burner in function of the error or “drop” in N2 due to the increase in

### 3 Structure of the simulation model

power demand in the way a droop governor does, as described by *MacIsaac and Langton* [20]. In addition, electrical power demand is commanded via the power demand block, where this is done in an analogous way to the original engine design, to recreate the effect of external aerodynamic effects on the rotor/output shaft absent in the model (different from those affecting ambient flow conditions to the engine).

#### 3.2.2 System block (Plant)

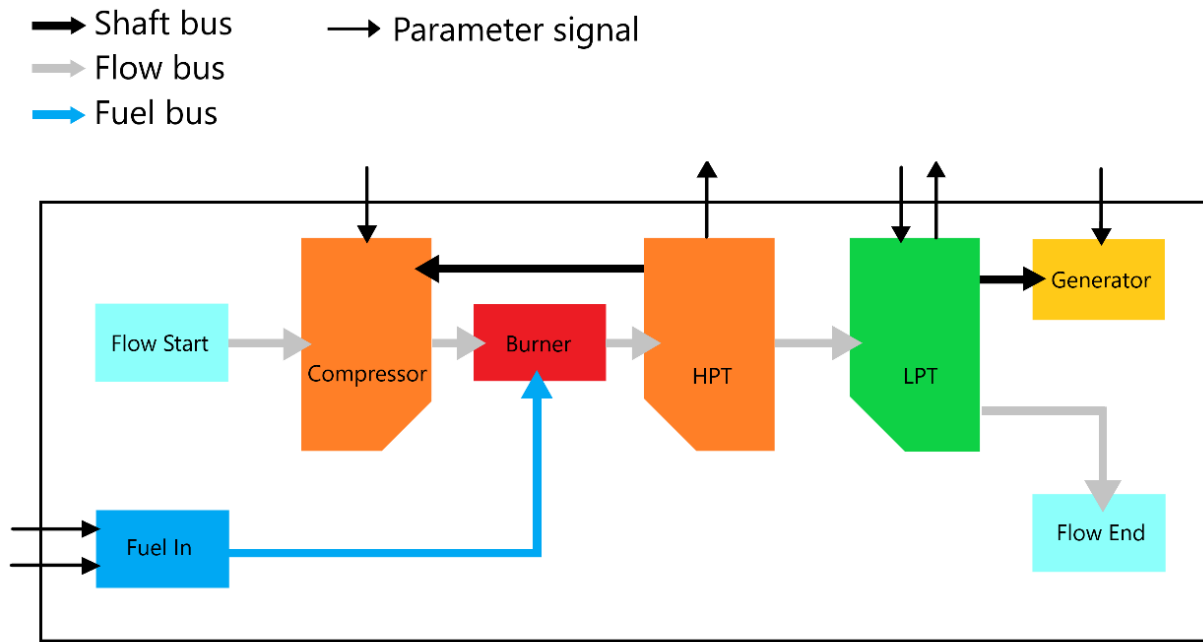


**Fig. 14. Allison M250 Model System Block**

The system block in Fig. 14 represents the plant in a conventional control loop and features the core engine components, the power shaft components as well as some of the auxiliary components. The system block is responsible for all flow and gas calculations as well as physical properties derived from the turbo-component maps.

The air and gas flow are incorporated into the design via Simulink® bus objects, with each bus carrying the signals of mass flow, temperature, pressure and velocity. The fuel bus also carries information on physical properties of the fuel, while the shaft bus holds data on mechanical power and rotational speed. The arrows for parameter signals represent each of the signals communicated by and to the adjacent blocks in the model.

The turbo-component maps are diagrams illustrating the operation field of the component and are usually extrapolated from experimental measurements that are conducted by varying the

### 3 Structure of the simulation model

different parameters of the component [17]. Fig. 15 shows a map of the compressor of the M250 during its investigation by *Marcellan et al.* [18]; the horizontal axis represents the corrected mass flow of working fluid through the component while the pressure ratio between the exit and entry pressure is plotted on the vertical axis. The solid black lines in the plot space represent the isotachs (constant speed lines) while the solid red lines depict constant efficiencies. In the example shown, a transient operation of the compressor is represented by the red operation points.

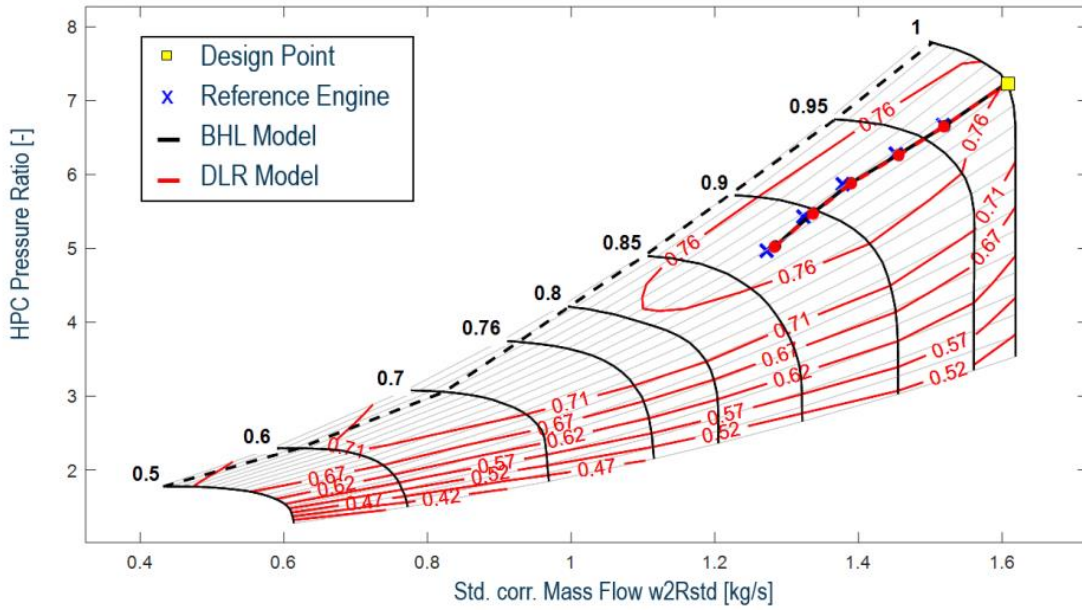


**Fig. 15. M250 compressor map with transient operation line [18]**

#### 3.2.3 Shaft-dynamics calculator block

The shaft-dynamics calculator block is responsible for computing the engine's shaft dynamics by applying power balance equations to the output of the system block with given inertia parameters of the shafts.

The shaft power  $P$  is defined in function of torque  $M$  and rotational speed  $N$  as [21]

$$P = M \cdot \omega = M \cdot N \cdot \frac{2\pi}{60} \quad \text{with } \omega = N \cdot \frac{2\pi}{60} \text{ the angular velocity} \quad \text{Eq. 3.1}$$

By applying the definition of torque  $M$  in function of moment of inertia  $I$  and the derivative of the angular velocity  $\frac{d\omega}{dt}$  [17]

### 3 Structure of the simulation model

$$M = I \cdot \frac{d\omega}{dt} \quad \text{Eq. 3.2}$$

the power balance equation is obtained

$$P = N \cdot I \cdot \frac{dN}{dt} \cdot \left(\frac{2\pi}{60}\right)^2, \quad \text{Eq. 3.3}$$

where  $N$  and  $I$  are respectively the rotational speed and the moment inertia of the corresponding shaft.

As a result of the uncoupled operation of the main engine shafts, the shaft-dynamics calculator block implements and computes the dynamics of each shaft independently. Concretely, based on Eq. 3.3, the rotational speed of the gas generator shaft is calculated as

$$P_{HP} = N1 \cdot I_{N1} \cdot \frac{dN1}{dt} \cdot \left(\frac{2\pi}{60}\right)^2. \quad \text{Eq. 3.4}$$

Similarly, by applying Eq. 3.3 to the power output shaft

$$P_{LP} = N2 \cdot I_{N2} \cdot \frac{dN2}{dt} \cdot \left(\frac{2\pi}{60}\right)^2. \quad \text{Eq. 3.5}$$

Eq. 3.4 and Eq. 3.5 are then solved with the initial values of  $N1$  and  $N2$  provided by the operator as well as the values of the moments of inertia of  $N1$ -shaft and  $N2$ -shaft, which represent a requirement to determine the initial state of the shafts. The initial rotational speeds usually depend on the operation mode of the engine, while the moments of inertia have been determined beforehand during the commissioning of the engine.

#### 3.2.4 MGTS<sup>3</sup> parameter study

The parameter study is a built-in tool of the MGTS<sup>3</sup> solver package that serves as an input interface with the Simulink<sup>®</sup> model. It is a MATLAB<sup>®</sup> structure array made up of intercommunicating tables, where each table like the one presented in Fig. 16 contains parameter properties and corresponding values which are distributed on cases that can be either activated or deactivated. General properties of the parameter study are also stored separately within the same structure.

### 3 Structure of the simulation model

<b>Parameters</b>	<b>Case 1 [active]</b>	<b>Case 2</b>	<b>Case3 [active]</b>	<b>...</b>
parameter 1	scalar	scalar	array	...
parameter 2	array	scalar	scalar	...
parameter 3	array	array	array	...
...	...	...	...	...

**Fig. 16. Parameter table of a parameter study**

The parameter study accepts two types of values for each parameter: either a scalar or unidirectional array. These values are then read by MGTS<sup>3</sup> internal functions that process the parameters based on their value to constant and variable parameters.

The resulting processed parameter study contains all the parameters in the form of variation arrays that combine of all the variable values with the constant ones. For example, if a parameter study contains two parameters, the first for the ambient temperature with the value of 273,15 K and a variation of the parameter XYZ contained in the MATLAB<sup>®</sup> array object [-1,1], the processing will result in the two variation arrays [273.15, -1] and [273.15,1].

The principle behind the use of a parameter study is the ability to prepare a simulative worksheet and apply it to the simulation successively without further interaction. Another reason is that the Simulink<sup>®</sup> model cannot be altered when in execution (Paragraph 3.2). Moreover, the simulation based on the processed parameter study uses a loop to iterate over the processed variations, which allows that the various parameters can be input in a safe manner without the need for exhaustive preprocessing. To further speed up the execution of the simulation, the constant parameters are sorted and fed before the simulation start so that only the variable parameters are overwritten after each Simulink<sup>®</sup> model execution.

## 4. Implementation of testing framework

### 4.1 Structure of the framework

The framework consists of a group of interconnected modules built as an add-on to the Simulink® model that is presented in Paragraph 3.2. Through the modular design of the framework, a communication with external libraries of MGTS<sup>3</sup> can be guaranteed.

The framework is an application from the structure discussed in Paragraph 2.3, where each of the modules serves one of the first three objectives of the evaluation architecture: synthesis, analysis, and optimization. The analogy between the original (left) and the implemented (right) framework structure is revealed in Fig. 17. Moreover, the original structure was not completely conserved but was instead applied specifically to the M250 simulation model using four substructures with alternative designations. In the following, the function of each substructure will be discussed individually.

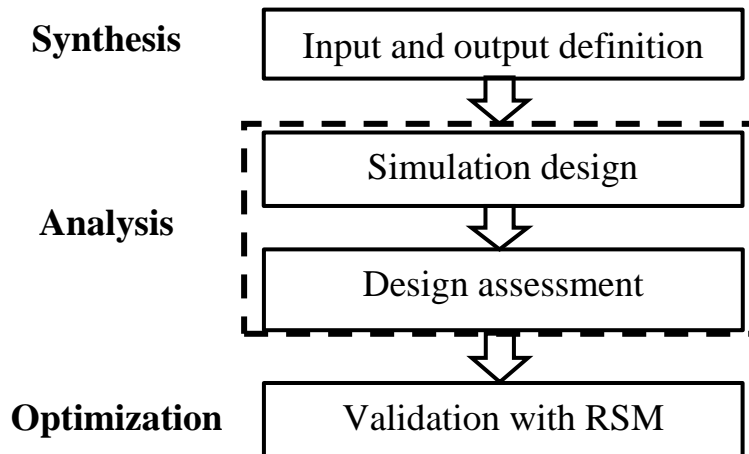


**Fig. 17. Application of the framework in the M250 model**

#### Input and output definition

The first task of the framework is the correct handling of the input from the user and its integration in the parametric study. Moreover, as part of this step, the necessary output of the simulation is defined according to the testing objective, e.g., output of values of N1 or N2.

### Simulation design

The second task is the correct processing of the input to a testing matrix. In concrete terms, the input is transferred to the parameter study to create a full factorial design (Paragraph 2.4.1), where the simulation run will iterate over each combination and execute it. The framework serves during this step as an interface between the user and the parameter study tool of the MGMTS<sup>3</sup> solver package, which itself communicates with the Simulink<sup>®</sup> model.

Inside the simulation loop, instantaneous postprocessing is required to extract the data from each execution based on the outputs defined, while more general postprocessing can be accomplished after the loop end. In the case of the framework developed in this work, the result of each simulation run is arranged in tabular form along with the combination of parameters used for that run after the simulation end, as this will speed up the processing in later steps.

### Design assessment

The third task of the framework is the analysis of the screening's results and the identification of the key factors from the simulation run for further investigation. This analysis is based on the evaluation of the system response by applying the criteria from Paragraph 2.2.

In a first step, the responses from factorial design will be validated using the time-domain characteristics of the signal, e.g., if a lack of convergence of the signal to its setpoint is detected, the response cannot be further fitted into a mathematical model as it would induce a great error, and thus is considered as invalid.

In a second step, the valid responses are used as a base for the mathematical model. In application of the steps proposed by Mee [22] in his guide for the two-level factorial design, the mathematical model used for the responses is that of a saturated model that includes all main and interaction factors. The saturated model describes a  $k^{\text{th}}$ -order regression (Eq. 4.1) where the saturated model response  $Y_{sat}$  is defined as function of all factors multiplied by a  $i^{\text{th}}$ -order regression coefficient  $b_i$  called intercept.

$$Y_{sat} = b_0 + \sum_{i=1}^k b_i x_i + \sum_{i=1}^{k-1} \sum_{j=i+1}^k b_{ij} x_i x_j + \cdots + b_{ij \dots k} x_i x_j \cdots x_k \quad \text{Eq. 4.1}$$

## 4 Implementation of testing framework

Moreover, no replication of the factorial design is needed due to the simulative nature of the model in this work, as any experimental error is absent and only a model lack-of-fit would be a source for error (Paragraph 2.3).

### **Validation with RSM**

The final task of the Framework is to validate the fitted model from the factorial design. By applying a *Box-Behnken* or a CCF design depending on the number of factors (Paragraph 2.4), the full factorial design can be augmented to a quadratic model, where confirmation runs can detect the curvature in the model and compare the error in the predicted and real responses.

## 4.2 Identification of key system parameters

The proposed design of the framework for the digital controller of the M250 needs to be validated before its implementation. To achieve this, it is necessary to identify potential key system parameters which could affect the stability of the controller. However, it is important to link the parameters to proven references, such as theoretical examinations or the experimental data generated by the commissioning of the M250 ground test rig at DLR, as it will be further discussed.

### 4.2.1 Theoretical background

The MGTS<sup>3</sup> solver mentioned in Paragraph 3.2.3 requires a set of defined start conditions for the working fluid. In the case of the M250, the variation of air ambient conditions outside the engine can lead to significant changes in the response of the system due to the heat and pressure losses [19]. The ambient flow conditions implemented in the simulation model are limited to the air temperature and pressure, which are taken into consideration as key system parameters.

In the simulation model, the thermal properties of fuel can also be varied. However, unlike the helicopter operation, the fuel conditions inside the laboratory where the M250 is mounted are strictly monitored due to preventive measures against the formation of explosive atmosphere in the laboratory. Accordingly, a variation of fuel properties has not been considered for the evaluation.



### 4.2.2 Experimental Background

After the introduction of the M250 engine as a demonstrator at the Institute of Combustion technology in early 2023, a measurement campaign was carried out to analyse the behaviour of the engine when coupled with the MGU as load unit. In Fig. 18, the transition from Ground Idle to Flight Idle is plotted, which was quite problematic in its first phase (greyed area). In fact, due to the quick change in the command value of N2 and the absence of a rotor inertia present in a helicopter package, the controller overcompensates the error by commanding an excessive fuel flow (orange line). In multiple cases, this has triggered an emergency shutdown of the engine due to N2-shaft overspeed.

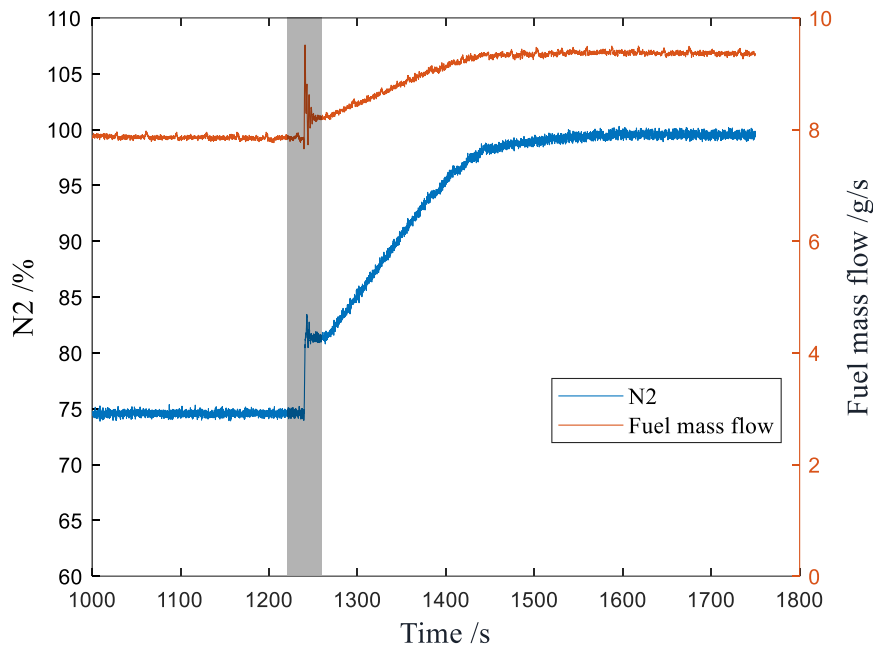


**Fig. 18. Transition from Ground to Flight Idle**

Since the fuel flow in the model is influenced by the value of the power demand of the MGU, which in return affects the value of N2 (Paragraph 3.2.1), the power demand has been added in the response investigation as one of the main factors that need to be properly compensated by the controller.

### 4.2.3 Literature reference

*Singh et al.* [23] developed a mathematical model for an SR-30 GTE with the purpose of developing a robust controller in a numerical model similar to that of the M250, especially in

## 4 Implementation of testing framework

the system components used. In this reference, the variables chosen for the start state vector are the compressor-exit pressure, the turbine-exit pressure and the output-shaft speed, whereas the rest of the parameters that are relevant for the thermodynamical system and the power balance are calculated based on the turbo-component maps.

Although the SR-30 is considered as a turbojet, its application within the test bench is analogous to the M250, as the thrust from the engine is converted using a free turbine to a mechanical power fed into an electrical alternator. Moreover, the work referenced makes use of experiment-based turbo-component maps that include a margin of error, which is equivalent to the approach implemented in the simulation model of the M250.

Furthermore, in his simulation of the performance of a two-shaft gas turbine, *Razak* [24] cites the deterioration of components as possible source for the error in the turbo-component maps, e.g., turbine creep, turbine blade erosion and overstressing of compressor blades and discs. As this error is not only key in the physical system, but also in the investigation of the controller performance, it was proposed that the efficiencies of the compressor, the HPT, and the LPT ( $\eta_{\text{comp}}$ ,  $\eta_{\text{HPT}}$  and  $\eta_{\text{LPT}}$  respectively) should be introduced as key system parameters that are to be varied during the analysis of the controller stability.

### 4.2.4 Case specific choice

Since the controller evaluation in this work revolves only around the operation phase of the M250 post Flight Idle, the control law is limited to the regulation of N2 as a function of the fuel flow. Due to the limitation imposed by the maximum turbine inlet temperature (TIT) and compressor's risk of surge [20], it is also important to implement the physical limits for the fuel flow in that of the controller. In the work of *Singh et al.* [23], this has been done using a saturation function, whereas in this work, the fuel flow limits were reverse calculated and implemented in the saturation output of the PI controller- block of Simulink® (see Fig. 19).

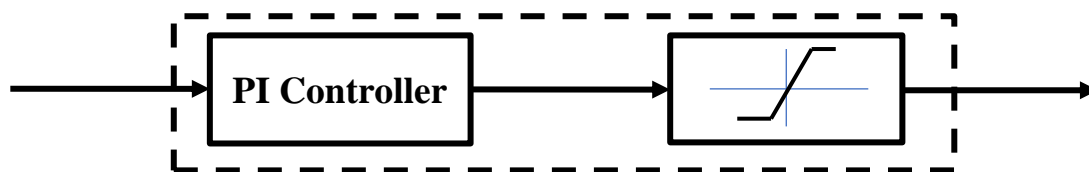


**Fig. 19. PI-controller block with output saturation**

## 4 Implementation of testing framework

Although the limits of the fuel flow supplied by the controller should be considered one of the key parameters, it was decided that the saturation range should not overshoot the current limitations of the FCS of the M250 and thus exclude it in the variation.

### 4.3 Parameter variation schemes

In the first phase of the work, the variation of parameters is divided into 3 different cases:

#### **Constant parameters**

The values of the parameters are constant throughout the simulation. They are initialised by the model or given a value by the operator. They also do not play any part in the preprocessing of the combinations.

#### **Steady-state variables**

The parameters are given a new value before each simulation iteration. These values correspond to the iteration being run and remain constant throughout the execution.

#### **Transient variables**

Like steady-state variables, the parameters are initialized with a new value, but it changes following a preconfigured transient shape throughout the execution of the model.

#### 4.3.1 Presentation of the parameters

Based on the observations discussed in Paragraph 4.2, several parameters are identified as potentially influencing the controller performance. In the following, an attempt will be made to link them with the model of the M250 and choose an appropriate variation scheme for each one.

The first parameter playing a role in the response of the M250 system is the power demand  $P_{el}$ . The power demand from the MGU controls the mechanical power output from the LP-shaft. By applying the power balance between the shaft and the MGU,  $P_{el}$  becomes the product of the torque of the shaft  $M$  delivered to the MGU and the angular velocity  $\omega$ . Additionally, if the electrical power demand  $P_{el}$  from the MGU is constant, it can also be defined as the voltage  $V_{MGU}$  of the MGU multiplied by the output current  $I_{MGU}$ .

#### 4 Implementation of testing framework

$$P_{el} = P_{LPT} = M \cdot \omega = V_{MGU} \cdot I_{MGU} . \quad \text{Eq. 4.2}$$

Eq. 4.2 demonstrates how it is possible in laboratory conditions to choose  $P_{el}$  for a determined steady-state respective of the MGUs variable electrical settings. In a real-life scenario of engine operation, the power demand is completely depending on the rotor dynamics and the transient aerodynamic effects acting on it. For example, strong wind gusts can result in a step-like behaviour of the power demand. For this reason,  $P_{el}$  will be varied as a transient variable during the operation.

Furthermore, the error in the turbo component maps elevated in Paragraph 4.2.3 leads to the next parameters that will be included in the response assessment, which are the isentropic efficiencies of turbo components  $\eta_{comp}$ ,  $\eta_{HPT}$  and  $\eta_{LPT}$ .

The isentropic efficiencies control the power extracted from the system and thus are also closely connected to the stability of the system. For the compressor, the isentropic efficiency is defined as the isentropic power  $P_s$  on the actual power  $P_a$  transferred to the flow, while for the turbine, it is the actual power  $P_a$  extracted from the flow on the isentropic power  $P_s$ .

$$\eta_{comp} = \frac{P_s}{P_a} \quad \text{Eq. 4.3}$$

$$\eta_{turb} = \frac{P_a}{P_s} \quad \text{Eq. 4.4}$$

The isentropic efficiency is implemented in the model as an affine transformation in the form

$$\eta_s = A \cdot \eta_{s,m} + B , \quad \text{Eq. 4.5}$$

where  $A$  and  $B$  represent respectively the linear coefficients and the translation of the theoretical isentropic efficiency  $\eta_{s,m}$  from the turbo-component map. The inaccuracy of the turbo maps discussed in Paragraph 4.2.3 is implemented to the system by varying  $A$  and  $B$  as a steady-state variable. In a variation of the linear coefficient  $A$ , a relative, physically-independent value is given. While by varying translation  $B$ , which is given as an absolute value, it does not require a definition of an initial value and thus can be added directly to the signal. In the variation of the three efficiencies, the linear coefficient will be varied.

## 4 Implementation of testing framework

After specifying the variation for the isentropic efficiencies, the next parameters that can affect the response of the system are ambient air pressure  $p_{\text{amb}}$  and air temperature  $T_{\text{amb}}$ .

The ambient air conditions represent, as mentioned in Paragraph 4.2.1, the initial values for the properties of the flow and each change in the surrounding conditions to the engine affects successively the flow in the latter stages. This on its turn affects the isentropic efficiency from the turbo-component maps and the power output of the engine. Since ambient conditions can change randomly depending on weather conditions on the day of the experiment, a steady-state variable is chosen for their variation.

### 4.3.2 Examination of transient signals

The behaviour in the transition from Ground Idle to Flight Idle discussed in Paragraph 4.2.2 is equivalent to a step-like increase in fuel mass flow, that when not met with enough load, can lead to overspeed state capable of damaging the engine. It was proposed that a similar transient phase should be simulated when testing the controller. In Simulink<sup>®</sup>, this would be characterized by an upward step in the power demand of the MGU.

Due to the restriction of the simulation model and its implementation in Simulink<sup>®</sup>, requiring that no simulation parameters can be varied during the simulation (Paragraph 3.2), the approach employed in creating signals for transient variables is the use of Multiport-switch blocks of Simulink<sup>®</sup> for each parameter. This type of switch enables the choice of signal shape between different cases, e.g., a step, a ramp, a quadratic signal, and the possibility to use a signal function, if suitable for the simulation case. The signal coming out of the Multiport switch in Simulink<sup>®</sup> is added to the original signal of the same parameter. This was designed to avoid initial value errors before the change in the signal. Most importantly, the parameters of this signal need to be defined by the operator in the input, where a special input function has been created for it.

## 4.4 Implementation of evaluation criteria

For the assessment of the FADEC in this work, the evaluation criteria introduced in Paragraph 2.2 will be applied to the operation phase of the M250 post Flight Idle. Hence, as mentioned in Paragraph 4.2.4, the chosen measured process variable is  $N_2$ , while the fuel flow  $\dot{m}_{\text{fuel}}$  is the output of the controller.

## 4 Implementation of testing framework

The evaluation criteria mentioned in Paragraph 2.2 are applied to N2 after the simulation run is finished. The used reference value is the design speed  $N2_{100\%}$ .

### 4.4.1 Time characteristics

For each type of the time characteristics enumerated in Paragraph 2.2.1 a MATLAB® function was created to process the discrete time response signal of N2 from the simulation.

First, the **rise time  $t_r$**  of the response is defined as the time required to reach 99% of  $N2_{100\%}$ . This rise time will be calculated respective of the nature of the parameter variation (steady-state/transient) from a chosen start time  $t_0$ . For example, if the rise time is large relative to the simulation execution time  $t_{end}$ , it implies a slow reaction to the response of the system.

The second measured characteristic is the **settling time  $t_s$**  which will be defined as the time taken to reach a bandwidth of 1% of  $N2_{100\%}$ . Analogously to the rise time, it will also be calculated from an initial instant  $t_0$ . Moreover, large settling time values can indicate an inadequate compensation of the response.

Third calculated will be the **overshoot OS**, which is defined in this case as the maximum positive signal error reached as a percentage of  $N2_{100\%}$  setpoint. An overshoot value of zero can indicate a good compensation but is only valid if the rise time and settling time are different from  $t_{end}$ .

### 4.4.2 Response curve criteria

As discussed in Paragraph 2.2.2, the response curve criteria will allow to earn a global idea of the evolution of the system response and complement the analysis done using the time-domain characteristics. A MATLAB® function processes the discrete time response signal of the speed of the output shaft of each parameter variation and compares it to the reference value  $N2_{100\%}$  to calculate the signal error. Moreover, for the calculation of the integral of each criterion, the infinite term is replaced by the simulation execution time  $t_{end}$  in Simulink®, e.g., for the ITAE criterion, the index  $Y_{ITAE}$  is defined as

$$Y_{ITAE} = \int_0^{t_{end}} t \cdot |e(t)| dt . \quad \text{Eq. 4.6}$$

### 4.5 Evaluation of sensitivity to disturbance

In Paragraph 2.3, the mentioned design for manufacturability aims to reduce the sensitivity of the response to global parameters. Since the power demand represents a disturbance parameter for the system that directly affects the command value of  $N_2$  due to the droop governor law [20], it is proposed to investigate the sensitivity of the system to the variation of this parameter in transient operation.

The qualitative investigation of the evolution of the system response to the variation of the disturbance parameter in this work is carried out to recognize singularities that are inside the factorial space. The reference factorial space in this work is the same used in the screening design (Paragraph 2.4.2). During the investigation, all other system parameters are kept constant, while the value of the power demand is incremented in small intervals. This would allow to understand the shape of the system responses in view of the interactions between the steady-state and the transient parameter, and detect the presence of any irregularities.

## 5. Validation of results and discussion

The validation of the parameters presented in Paragraph 4.2 and the evaluation of the controller performance in compensating the effects of these parameters is carried out by the framework illustrated in Paragraph 4.1. During this chapter, each of the building blocks of the framework will be presented through a concrete example of a simulation run designed like a real test of the FADEC. Subsequently, the results will also be examined and discussed in terms of validity.

### 5.1 Test case

The example presented during this chapter is that of the variation of the six parameters  $P_{el}$ ,  $\eta_{comp}$ ,  $\eta_{HPT}$ ,  $\eta_{LPT}$ ,  $p_{amb}$  and  $T_{amb}$  presented in Paragraph 4.2 as steady-state parameters as well as the introduction of a step for the power demand  $\Delta P_{el}$  at a time  $t_{step}$  of the simulation as a transient parameter. Moreover, the constant parameters  $N1_{init}$  and  $N2_{init}$  are also provided since they are required by the shaft-dynamics calculator to determine the initial state of the shafts (Paragraph 3.2.3).

#### 5.1.1 Input and output definition

In this first section, a two-level full factorial design based on seven variable factors is carried out for the test. The execution time of each run is  $t_{end}$ , with a Simulink® discrete timestep of 0.1 s. The choice of the timestep was based on trial runs, where the timestep was reduced until no significant deviations in the system response were observed for the same system input.

For the uniformity of the results of the factorial design,  $t_{step}$  must remain constant through all treated combinations. Consequently, a  $t_{step} = \frac{t_{end}}{2}$  was chosen as the instant for the step input. Using the simulation halftime ensures that the probability of a steady-state instability is split on two. On one hand, if the setpoint convergence is not reached before the step input, the effect of this instability will still be observed due the new change in setpoint value. On the other hand, if a steady state is reached, only the effects of the transient input will be observed in the simulation result. It is also worth noting that this probability is only considered when evaluating the response with time-domain criteria, as the response curve criteria are not sensitive for time settings.



## 5 Validation of results and discussion

As a most appropriate scenario for the eventual real test of the M250, the two levels of  $P_{el}$  should represent the vertices of the shaft power output. For this, the engine ratings at Flight Idle and at 100% Maximum Cruise represent good candidates (the Maximum Take-off engine rating being only intended for limited use and will not make a part of the test of the controller in the scope of the WET-integration).

Accordingly, the parameter study shown in Table 5.1 was split into two separate cases, which also include the Simulink® step-block variables for the variation of the shaft power as a transient variable with two vertices of the step given as the variable  $\Delta P_{el}$ . However, due to an inconsistency of the engine model with the real model, where the characteristics of the compressor air-bleed valve were not properly integrated, it has been observed that the 100 % Maximum Cruise rating given by the manufacturer cannot be exceeded. Moreover, as the value of  $\Delta P_{el}$  coming out of the Step-block in Simulink® is added to the original value of  $P_{el}$ , a corrected rating needed to be used, where the maximum value of  $P_{el}$  at 100 % Maximum Cruise is never surpassed.

**Table 5.1. Parameter study of the investigated case**

Parameter	Case: Flight Idle	Case: Corrected Maximum Cruise
$P_{el}$ /W	26 000	146 000
$\eta_{comp}$	[0.85;1.15]	[0.85;1.15]
$\eta_{HPT}$	[0.85;1.15]	[0.85;1.15]
$\eta_{LPT}$	[0.85;1.15]	[0.85;1.15]
$p_{amb}$ /Pa	[97 500;101 500]	[97 500;101 500]
$T_{amb}$ /K	[273.15;303.15]	[273.15;303.15]
$N1_{init}$ /rpm	36 114	51 180
$N2_{init}$ /rpm	33 290	33 290
$t_{step}$ /s	15	15
$\Delta P_{el}$ /W	[5 000;20 000]	[5 000;20 000]

Additionally, after observing the values of the isentropic efficiencies that should be used, based on the uncertainty of  $\pm 15\%$  used in the work of *Singh et al.* [23] and discussed in Paragraph 4.3.1, it was decided to further decrease the maximal power demand. In fact, as the total efficiency of the system depends on the isentropic efficiencies of the two turbines and the compressor, a combination of efficiency loss in these three components would result in a very

## 5 Validation of results and discussion

low power output [17]. Hence, based on some test runs, a maximum value of 146 000 W was chosen for  $P_{el}$ .

For the ambient air conditions, the ranges of the absolute barometric pressure range and temperature were chosen as approximates to the average local values for the city of Stuttgart [25]. The average pressure value chosen is 99 500 Pa with a correction of  $\pm 2\,000$  Pa and the average temperature value chosen is 15 °C (288.15 K) with a margin of  $\pm 15$  °C.

### 5.1.2 Simulation design

Using the input/output modules of MGTS<sup>3</sup>, the processed parameter variation yields a full factorial design containing  $2^7 = 128$  combinations. These combinations are iterated over and executed with the Simulink<sup>®</sup> model. Table 5.2 shows how the values are coded (or scaled) in the full factorial design in analogy to the reference mentioned in Table 2.1.

**Table 5.2 Coded values for each variable parameter**

Parameter	Coded minimum: -1	Coded maximum: 1
$P_{el} / \text{W}$	26 000	146 000
$\eta_{\text{comp}}$	0.85	1.15
$\eta_{\text{HPT}}$	0.85	1.15
$\eta_{\text{LPT}}$	0.85	1.15
$p_{\text{amb}} / \text{Pa}$	97 500	101 500
$T_{\text{amb}} / \text{K}$	273.15	303.15
$\Delta P_{el} / \text{W}$	5 000	20 000

For a better coherence, only the coded values of the parameters will be used in the further progression of this chapter, referred to as minimum or maximum, as well as minimal value or maximal value.

## 5.2 Result of the full factorial design

To exploit the results of the full factorial design, the first order effects of each factor in the design on the response of the system will be observed to validate the key factors and extract a first order model that will be validated with an RSM design. But first it is proposed to discuss the response from the different runs qualitatively.

## 5.2.1 Qualitative assessment of results

It is important to first analyse the evolution of N2 in function of time and the system parameters. The plots in Fig. 20 show this evolution where the results are divided into four groups corresponding to a combination of a constant values for  $P_{el}$  and  $\Delta P_{el}$ , e.g.,  $(P_{el}, \Delta P_{el}) = (-1, 1)$  (in coded values), while the other parameters are varied between their minimum and maximum. Each of the groups are represented by a plot in the same figure. Moreover, for clarity purposes, each curve corresponding to a simulation run has a separate colour.

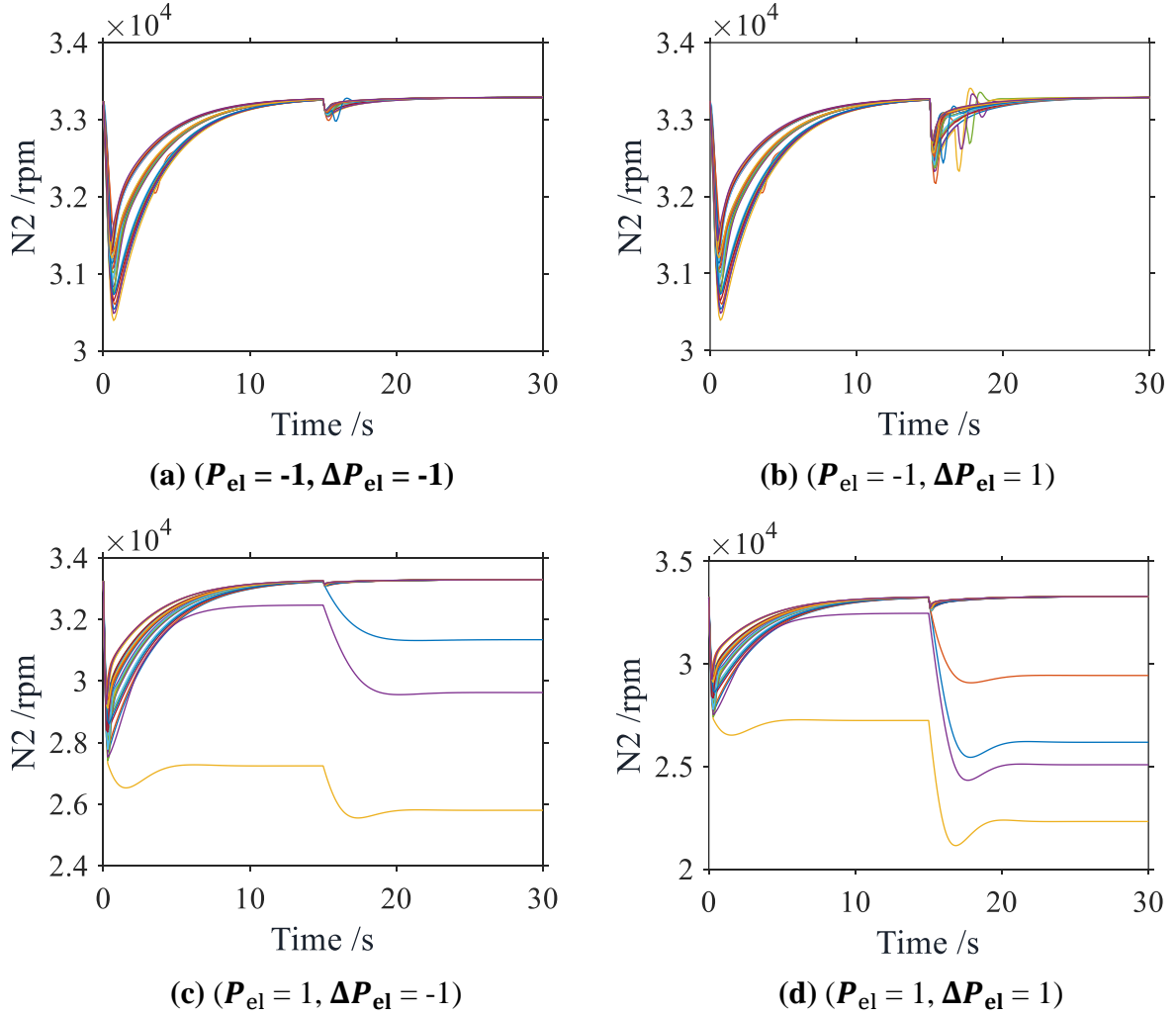


**Fig. 20. Variation of N2 as a function of time,  $P_{el}$  and  $\Delta P_{el}$**

## 5 Validation of results and discussion

Due to the nature of the test case, it is preferable to segment the analysis into two segments. In a first time, it is proposed to study the steady-state response of the system, characterized by the response up to 15 seconds. In a second time, the succeeding transient phase is considered.

In the first half of the simulation, an initial, relatively small drop in the value of  $N_2$  is observable in all plots, that is in some cases either followed by an ascent to the setpoint, or a further drop to a stable  $N_2$  value different from the original setpoint. This different value represents a different equilibrium state of the system (which can also be a state of immobility of the shaft). It is also observable, that in the case of  $P_{el}$  at its minimum value (see Fig. 20-a, -b),  $N_2$  always converges to its command value, with almost no oscillations present in the first half of the response. This is however does not fully apply for the maximum level.

The second half of the simulation represents the response of the system after the step input in the power demand is introduced. The resulting effects of this transient change are diverse, but can be divided into three main categories:

### **Instant distortion followed by a setpoint convergence**

Considered as best response scenario, the step change only triggers a small drop in  $N_2$  that is quickly compensated by the controller where  $N_2$  merges with its original value. This effect is observable for all treated combinations where  $P_{el}$  is at a minimum and some combinations where it is maximal. Interestingly, in some specific cases, the compensation is characterized by a limited oscillation due to the combination of parameters, although this phenomenon will not be further analysed. Moreover, this first scenario also includes some of the cases where a new equilibrium is established, and where a successful compensation occurs.

### **Partial loss of speed**

The second scenario after the step change is a partial drop in  $N_2$ , which is usually preceded by a not-fully-established steady-state. Like the effect present at the first half of the simulation, this indicates an establishment of a new equilibrium in the system, where the power output is supplied at a lower rotational speed but at a higher torque.

### **Complete loss of speed**

The last response scenario concerns only the combinations for  $P_{el}$  is a maximum, where even

## 5 Validation of results and discussion

after the establishment of an alternative setpoint in the first half of the simulation, N2 drops to almost zero after the step input.

To sum up, the analysis of the N2-system response shows that two different scenarios result from the variation of steady-state parameters, while three scenarios result from the transient change. Nevertheless, it is important to note that in the real thermodynamic cycle, a sole equilibrium dictated by the N2 setpoint is preferred for a certain combination of parameters. This is why responses where an alternative equilibrium is reached will be considered as invalid simulation results.

### 5.2.2 Validation of the different runs

For the evaluation of the N2-response of the system to the varying parameters, both types of criteria discussed in Paragraph 4.4 will be exploited. While mainly the ITAE criterion from the response curve parameters and the settling time criterion from time-domain criterions will be used, other discussed criteria will be introduced and compared briefly.

As mentioned at the end of Paragraph 5.2.1, an initial filtering must be carried out to select valid responses by applying the settling time criterion. This is necessary for the mathematical model that will be based on the comparison of the responses with the ITAE criterion. The settling time  $t_s$  will be also used for comparison, however, due to the presence of the two steady- state and transient phases, this criterion cannot give generalized results for the screening design.

The behaviour of the system responses is presented in Fig. 21 in terms of convergence in each of the steady-state and the transient domains. In both plots, the rise time  $t_r$  and settling time  $t_s$  are applied as evaluation criteria. However, it is important to discuss this application before looking at the results.

#### **Setpoint droop**

As elaborated in Paragraph 4.4.1, the time-domain criteria are calculated from an instant  $t_0$  where a setpoint variation takes place. In our case however, there is only a virtual setpoint variation happening, this is due to the nature of the droop governor control law in Post Flight Idle operation of the M250, where the controller compensates a finite control error from a constant setpoint N2<sub>100%</sub>. While the instant at which  $P_{el}$  is varied can be considered as a good

## 5 Validation of results and discussion

candidate for  $t_0$ , e.g.,  $t_{\text{step}}$ , it can sometimes lead to an erroneous measurement, e.g., in the case of a small decrease in  $N_2$ . For this reason, the instant  $t_0$  chosen for calculating the criteria, is the moment at which the control error reaches a maximum and starts decreasing.

By analysing the results from both criteria, one can on one hand compare the steady-state convergence of the signal, and on the other hand evaluate the substantiality of the effect of the transient operation.

In the steady-state domain, if the settling time  $t_s$  is equal to  $t_{\text{step}}$ , it can be concluded that up to the step input  $\Delta P_{\text{el}}$  the system did not reach a valid steady-state where the  $N_{2100\%}$  setpoint is attained. The same rule applies for the transient domain, however with  $t_{\text{end}} - t_{\text{step}}$  (as a difference) instead of  $t_{\text{step}}$ . This can be deduced visually from the plots by the number of peaks that go up to the edge of the plot, where there are three more cases in transient domain where simulation runs lead to a rotational speed other than  $N_{2100\%}$  than in steady-state domain. It is also worth noting, that the figure confirms the results of the qualitative assessment in Paragraph 5.2.1 by hinting the structure of the full factorial design, where the first half of the runs, represent the combinations where  $P_{\text{el}}$  is minimal, and where the response is more uniform.

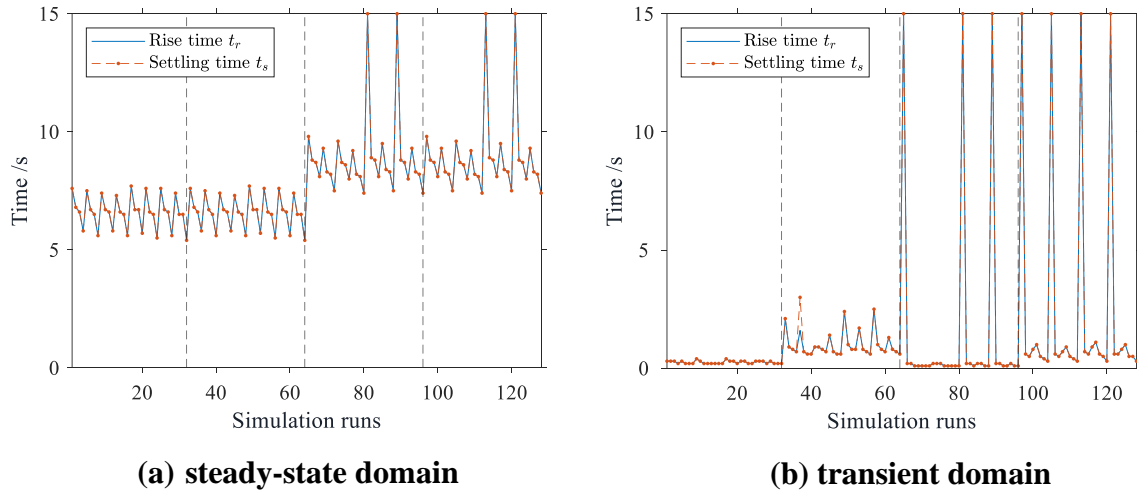


**Fig. 21. Comparison of the time-domain**

By further splitting the plots of the figures into 4 regions in an analogous manner to the qualitative assessment in Paragraph 5.2.1, is also possible to analyse the dynamics of the signal evolution.

### Region 1: Simulation runs from 1 to 32

In this region, the calculated values for  $t_r$  and  $t_s$  are equal and are at a minimum in both domains. This indicates a low-oscillating convergence, where the amplitude of oscillations remains in a *margin* of 1 % of the setpoint, which can result in a coincidence with the rise time that is also calibrated to 99 % of the setpoint. As for the second half of the simulation, residual values of  $t_r$  and  $t_s$  indicate that the step input always have *marginal* effect, inducing a small control error that is compensated in under 1 second from  $t_{\text{step}}$ .

### Region 2: Simulation runs from 33 to 64

In this sector, the values of the two  $t_r$  and  $t_s$  remain almost unchanged from the previous sector in the steady-state domain. However, in the transient domain,  $t_r$  and  $t_s$  both increase in value, showing a delay in compensation up to 2.5 seconds. Moreover, a single case where  $t_s$  is higher than  $t_r$  is present, indicating an oscillation that exceeded the bandwidth of 1% of the command value of N2 (see Fig. 20).

### Region 3: Simulation runs from 65 to 96

In the third region, there is a presence of invalid runs indicated by a  $t_s$  that is equal to  $t_{\text{step}}$  or  $t_{\text{end}}$  depending on the domain. Furthermore, the effect of the increased  $P_{el}$  resulted in a longer  $t_s$  by almost 3 seconds compared with the previous regions of the plot. This increase in  $t_s$  however, is not propagated to the transient time, where only shorter  $t_s$  are seen. Nevertheless, an additional case where the introduction of the step input was responsible for the divergence from the setpoint is present, highlighting the combined effect of  $P_{el}$  and  $\Delta P_{el}$ .

### Region 4: Simulation runs from 97 to 128

In this last quarter of the simulation, the combined effect of  $P_{el}$  and  $\Delta P_{el}$  observed in region 3 is more consistent where two additional cases of failed compensation arise in the transient domain compared to the steady-time domain. Additionally, similar to region 2,  $t_r$  and  $t_s$  witness a small increase in their values.

To conclude this analysis, using the time-domain criteria and the dissection of the full factorial matrix in 4 comparable regions, it was possible to earn an impression of both the individual and

combined effects of  $P_{el}$  and  $\Delta P_{el}$  on the temporal dynamics of the signal. However, to understand and compare the effects from all factors, a mathematical approach will be employed.

### 5.2.3 Comparison of the evaluation with response curve criteria

Before investigating the individual factors, it is worth studying the differences of the different response curve criteria mentioned in Paragraph 2.2.2.

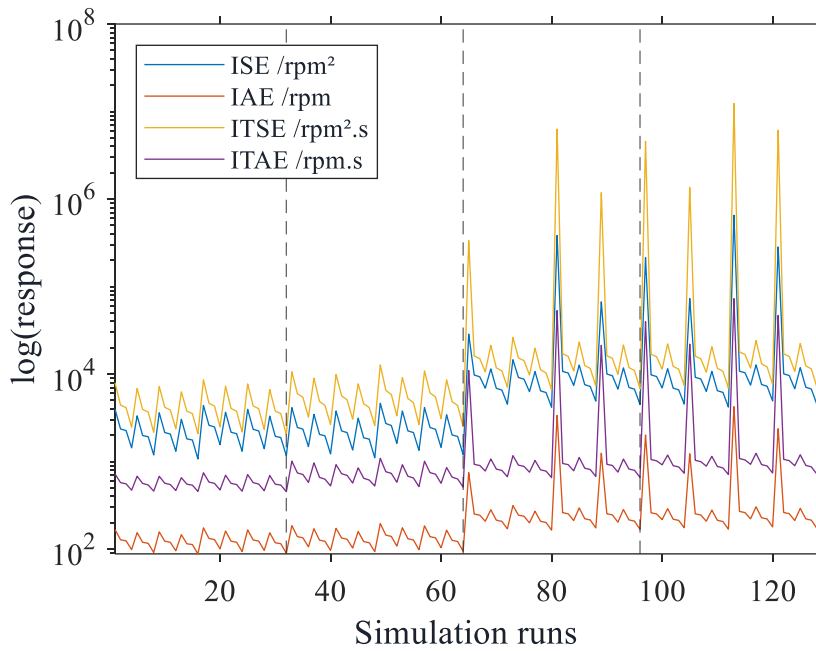


**Fig. 22. Response curve criteria comparison**

A comparison of the various methods is proposed in Fig. 22. The purpose of this comparison is to display which method can be most suited to the evaluation in progress without looking at the specific structure of the test case.

The shape of the curves for the different methods confirms the mathematical prognosis from Paragraph 2.2.2 of the characteristics of each method. In fact, in analogy to the dynamic behaviour assessment, the time integral criteria ITSE and ITAE highlight the difference in the response magnitude of the set of runs from 1 to 32 and the set of runs from 33 to 64. Moreover, due to the quadratic nature of the integral term, it is noticeable how ISE and ITSE methods significantly help highlight small differences in the calculated criteria values from run to run, that remain undetectable especially when using a logarithmic scale plot.



## 5 Validation of results and discussion

In the further progress of this evaluation, it has been decided to use the ITAE as a most efficient evaluation criteria, that also would not yield exaggeratedly large results.

### 5.2.4 Results of the full factorial design

The main target of the full factorial design as a screening test is the comparison of parameters to determine their effects on the response. After the conclusion of simulation, the responses from each combination are calculated by applying the ITAE method to the measured signal of N2.

Determining the effect  $Y_{\text{effect}}$  of each parameter consists in measuring the difference between the average response values at each of the vertices of the parameters (see Fig. 10). This is given by the following formula

$$Y_{\text{effect}} = \frac{\sum_{i=2}^k Y(+1, x(i)) - \sum_{i=2}^k Y(-1, x(i))}{n_{\text{comb}}}, \quad \text{Eq. 5.1}$$

where  $k$  is the number of factors and  $x(i)$  represents the coded value for each remaining factor different than the factor fixed by -1 or 1, while  $n_{\text{comb}}$  represents the number of the combinations.

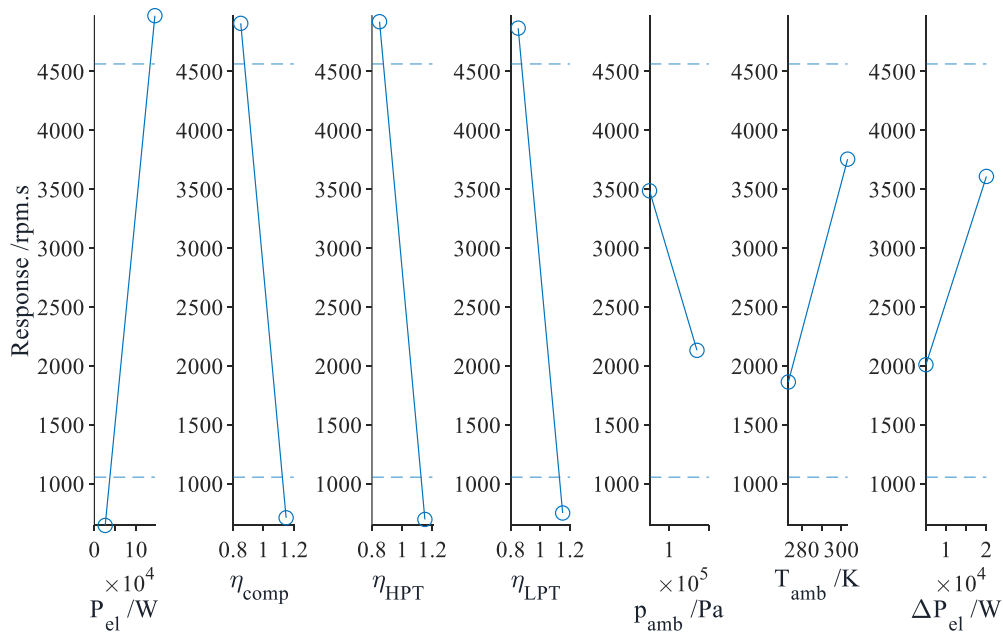


**Fig. 23. 1<sup>st</sup> Order effects of the full factorial design using ITAE criterion.**

## 5 Validation of results and discussion

The first order effects of the full factorial design are plotted in Fig. 23. The solid lines represent the effect magnitude of each factor, while the dashed lines show the standard deviation of these magnitudes. The standard deviation is a criterion to compare each factor's effect with the average value of all effects  $\bar{Y}_{effect}$  and is given by the formula

$$\sigma = \sqrt{\frac{\sum (Y_{effect} - \bar{Y}_{effect})^2}{n_{comb}}}. \quad \text{Eq. 5.2}$$

### 5.3 Assessment of the response model

Looking at the standard deviation of the effects from Fig. 23, it is noted that the effect of the power demand and all isentropic efficiencies of the turbo components is dominant, with that of the power demand having a slightly larger magnitude. It is also worth noting that the isentropic efficiencies along with the ambient pressure have a reverse effect on the response of the system, e.g., in the case of the LPT, a minimal value for the isentropic efficiency results in a deficient response, which coincides with the physical effect of the high component deterioration discussed in Paragraph 4.2.3.

In a second step, a mathematical model is developed using a first order linear regression and a full linear regression of the results of the full factorial design (Eq. 4.1). More specifically, the model is also based on the coded values of the parameters, so that the physical properties of the factors are not included in the coefficients.

Furthermore, as brought forward in Paragraph 5.2.1, response filtering is necessary to create a correct regression model, as the presence of outliers in the model can cause an increased value of the intercepts resulting in a model lack-of-fit. Additionally, by applying a confidence level to coefficients of the first order regression corresponding to each factor of the model [15], they are evaluated by their absolute value and compared to the observations from the standard deviation.

The result of this methodology is illustrated in the pareto plots in Fig. 24 . The nature of this plot allows to visualize the coefficients making up the sum up to the chosen confidence interval of 95 % with their absolute values sorted on a histogram from largest to smallest.

## 5 Validation of results and discussion

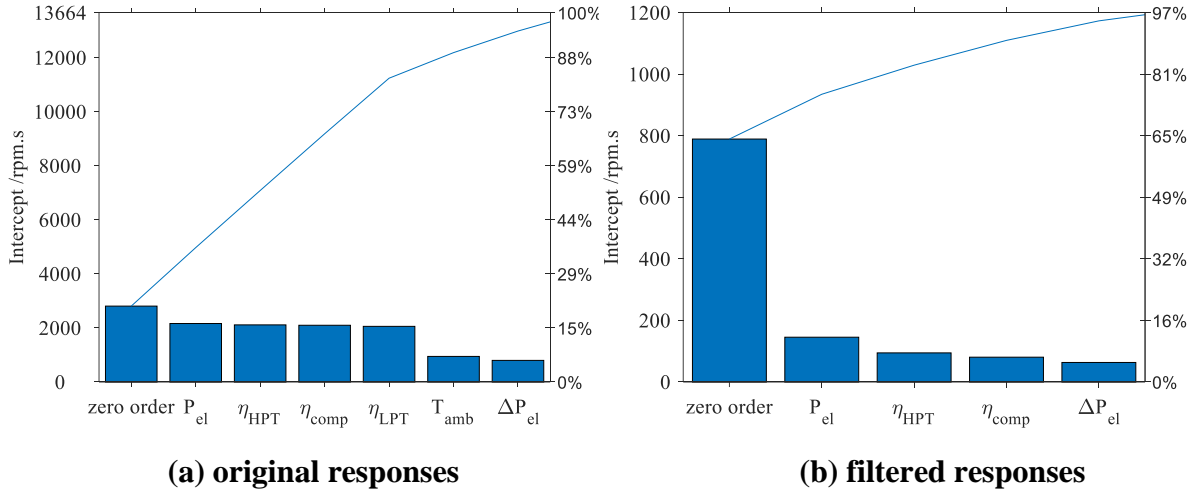


**Fig. 24. Intercepts from linear regression**

When comparing the intercepts from the results of the full factorial design and those after filtering, a difference in the absolute value of the coefficients making up the confidence interval is observed. While the magnitude of this difference depends on the response curve criteria used, it can be explained by the presence of the outliers, that broaden the value range of the responses.

The left plot showing the first order fitting from the original responses highlights that the largest regression coefficients coincide with the largest effects from the full factorial (Fig. 23), where the power demand and the isentropic efficiencies dominate in magnitude. However, the regression coefficients from the filtered results mark the presence of other key coefficients, such as  $\Delta P_{el}$  that outweigh other coefficients such as  $\eta_{LPT}$  when only valid responses are considered.

Furthermore, another different aspect between the two plots is in the values of the zero-order coefficient when compared to other intercepts. This value, resulting from the intrinsic presence of the initial drop in the response curve of N2 (Paragraph 5.2.1), indicate that in the filtered responses, the initial drop has a more significant effect compared with the system parameters.

In the following, it is opted to use the regression model from the valid responses. By employing the results from the plot, a reduced first order model of the response  $Y_{red}$  can be created, with the following expression

$$Y_{red} = 798,5 + 145,51 \cdot x_{P_{el}} - 94,5 \cdot x_{\eta_{HPT}} - 80,6 \cdot x_{\eta_{comp}} + 63,4 \cdot x_{\Delta P_{el}} \quad \text{Eq. 5.3}$$

Subsequently, the results of the reduced model and the first model are compared it to the valid responses of the full factorial (see Fig. 25). From the evolution of the response, it is possible to distinguish the four different regions discussed in the qualitative assessment Paragraph 5.2.1, where the model succeeds in following the transition from one domain to the next. However, it is also noticeable how an estimation error from both mathematical models is spread on the entire domain, although being larger for the reduced model. In general, this error lets to conclude that first order fit is not adequate for correctly estimating the responses.

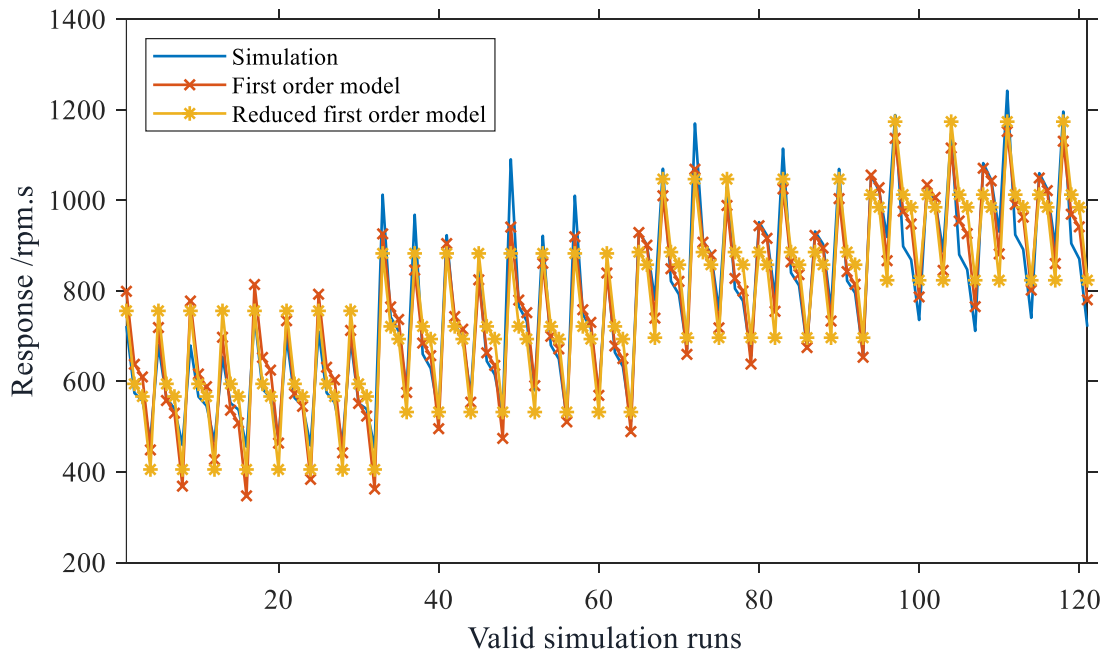


**Fig. 25. First order model and reduced model comparison to the results of the full factorial.**

### 5.4 Augmentation of the response model with RSM

In the next step of the assessment of the performance of the controller, it is relevant to diagnose the limitations of the full factorial design and to understand the evolution of the responses inside the factorial space, as the full factorial design only covers its vertices. Using RSM, it would be able to validate the model of the responses with the responses from axial points on the surfaces of the factorial space (see Fig. 11 for reference).

The application of a *Box-Behnken* design as an RSM model can cost unnecessary extra time as the design itself is only efficient for a total number of factors under four, as stated in Paragraph 2.4.2. Moreover, due to the already executed full factorial design, it is optimal in this

## 5 Validation of results and discussion

case to augment it to a CCF design, where the response of the axial points can be used to evaluate the accuracy of the full regression.

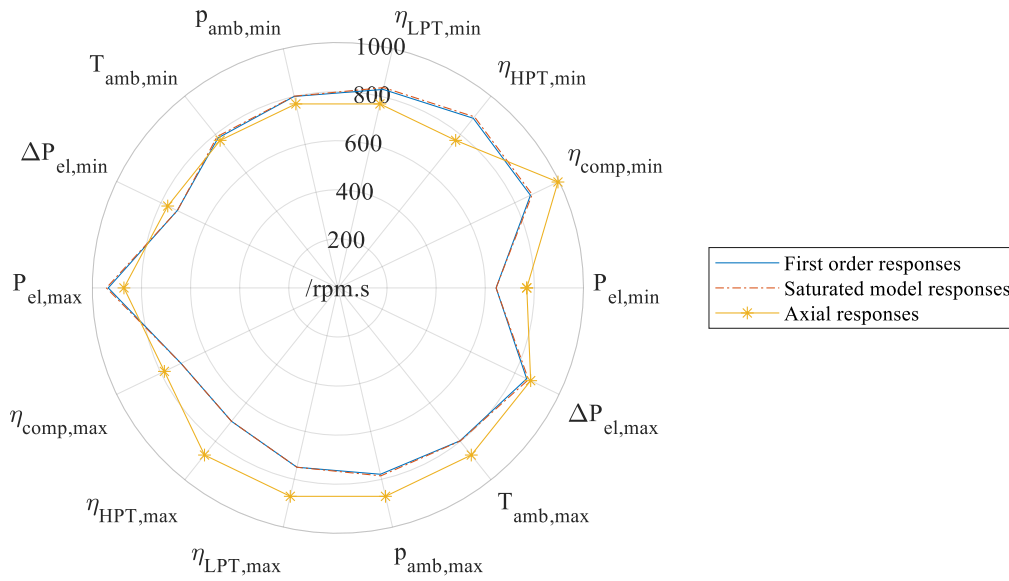


**Fig. 26. Comparison of responses from first order model, saturated model and from axial points**

The responses of the axial points represent the effects associated with points inside the variation range of the parameters that cannot be detected by the full factorial design. The axial points are in this case  $2 \cdot 7 = 14$ , where in each combination one parameter is given one of its extreme values, while the others are set to their midrange values. The distribution of the difference on the different parameters is illustrated in Fig. 26. The radial distance between the lines gives an idea of the real curvature of the response function inside the parameter range of the parameters.

From a first view, the comparison of the first order model and the saturated model shows no difference in the values of the responses. This is most importantly due to the nature of the coded axial points in the mathematical model that give a value of zero for midpoint value of a factor. The coded regression used in this case is essential to obtain a simplified model that can be easily investigated [22]. This also means that no difference can be observed between a first order and a seventh order model, like the one representing the saturated model in this case.

On another side, it is interesting to note from the polar distribution how for most parameters, the response from the mathematical models is underestimating the real responses. This aspect indicates a conservative behaviour of the system inside the factorial space, which is the space separating the vertices of the parameters. This does also mean that some of the parameters need

to be investigated closely, either by using other RSM designs or by evaluating the concerned factors in singular runs.

### 5.5 Analysis of the disturbance effect of power demand

In this last part of the evaluation, it is proposed to further extend the framework evaluation architecture with an evaluation of the system disturbance. It is worth mentioning that in this case, the disturbance itself must be included in the simulation model of the engine and correctly identified by the operator, using the evaluation framework for example. However, once this identification is accomplished, this extension would allow to implement this parameter as a disturbance factor and analyse it distinctively from all process parameters.

Similar to the test of transient conditions from Paragraph 5.1, a test case for the parameter can be input in the parameter study, where it is configured to only test the disturbance itself.

#### 5.5.1 Test case

This example analyses the effect of the power demand  $P_{el}$ , which represents a very volatile parameter that can be affected by aerodynamical effects and different flight conditions. Using the transient step input in power demand  $\Delta P_{el}$ , the intention is to understand the shape of the evolution of the response to the variation of this parameter.

The test case used is based on the case “Flight Idle” from Table 5.1. However, all parameters apart from  $\Delta P_{el}$  were given their minimum values (see Table 5.2). It is also worth noting that  $\Delta P_{el}$  was varied in small intervals from the same minimal to the same maximal value from Table 5.2, as it is plotted in Fig. 27.

The approach in using already exploited values for the parameters allows to avoid any invalid output from the design, due to the low setting of  $P_{el}$  and enables the comparison of the created mathematical model with the results from the simulation (see Paragraph 5.2).

### 5.5.2 Qualitative analysis

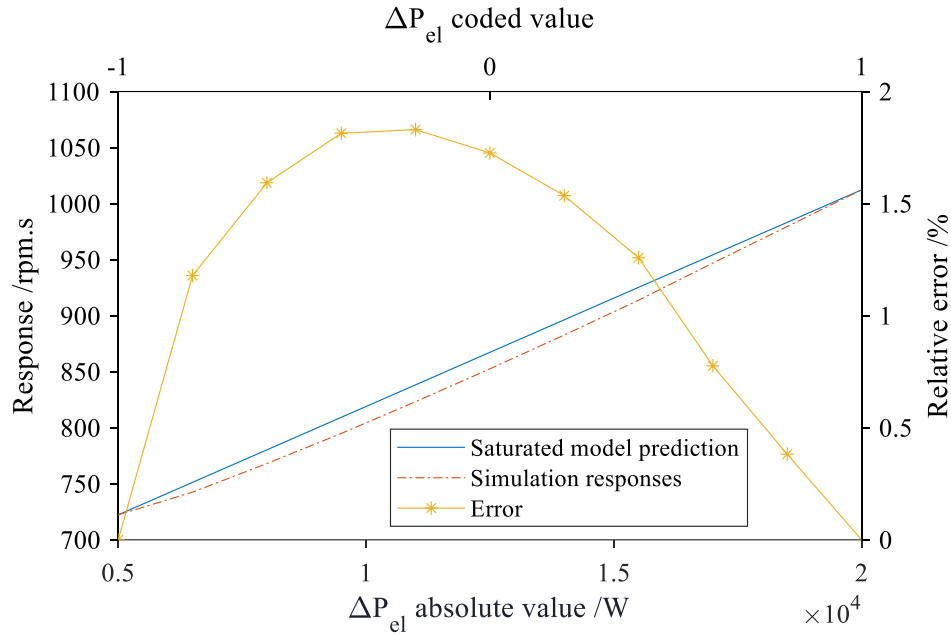


**Fig. 27. Variation of the power demand as a disturbance parameter**

The evolution of the responses evaluated using ITAE criterion in Fig. 27 presents a continuous aspect that does not feature any irregular values. This indicates that in the case of a low power setting, even with a high rate of component deterioration, the slow variation of the load on the engine is compensated by the controller.

Furthermore, by comparing the saturated model from Paragraph 5.1.2 and the results of the simulation, an error margin that varies in amplitude across the range is observed. While the full fitted model predicts a linear behaviour, this error indicates a curvature of the response behaviour that is annulled at the edges of the variation range.

These observations give a good idea about the shape of the response curve between the vertices of the design, and thus allow to refine the input range for the different parameters after identifying their effects, to achieve optimal experimental results.

## 6. Summary

During this work, it has been possible to apply the methodology of control-loop testing and Design of Experiment, to construct an efficient structure for the framework to test the FADEC of the M250 engine. The entire package of the framework is integrated within the simulation package and does not include any external components.

The architecture of the framework enables to investigate multiple scenarios by dynamically varying the system parameters, evaluate and validate the effect of key parameters on the controller performance, extract a mathematical model for further testing with same scenario parameters, and finally analyse parameters individually within a custom range.

Moreover, although the identified key parameters in this work are limited to the current engine model, the framework is not limited to the model itself and any later expansion of the model can be reevaluated for other key factors. This versatility in the testing of parameters can prove advantageous to the planned HIL testing phase and the later integration of the components for the WET cycle.

### Outlook

The parameters identified in this work for the evaluation of the system response were based on real parameters that are also included in the MGTS<sup>3</sup> simulation model of the engine. With the evolution of the model and the inclusion of other effects such as heat transfer, that would itself affect the turbines, new framework assisted identification may be required.

In addition, in what regards the physical testing, the FADEC will be installed on a speedgoat® real time target machine and connected to the real controlling system. During this phase, real effects that are associated with the controller like control delay can be implemented in the framework by updating the evaluation criteria.

Finally, the framework will help achieve the goal of reducing the risks accompanying the commissioning of the digital controller implemented in the WET-demonstrator.



## 7. References

- [1] Schmitz, O., Kaiser, S., Klingels, H., Kufner, P., Obermüller, M., Henke, M., Zanger, J., Grimm, F., Schuldt, S., Marcellan, A., Cirigliano, D., Kutne, P., Heron-Himmel, A., Schneider, S., Richter, J., Weigand, B., Göhler-Stroh, A., Seitz, A., and Hornung, M., “Aero Engine Concepts Beyond 2030: Part 3—Experimental Demonstration of Technological Feasibility,” *Journal of Engineering for Gas Turbines and Power*; Vol. 143, No. 2, 2021. doi: 10.1115/1.4048994.
- [2] Rolls-Royce plc, *M250 Engine Information*, 2023.
- [3] Federal Aviation Administration, “Rotorcraft flying handbook,” 2000, [https://www.faa.gov/sites/faa.gov/files/regulations\\_policies/handbooks\\_manuals/aviation/faa-h-8083-21.pdf](https://www.faa.gov/sites/faa.gov/files/regulations_policies/handbooks_manuals/aviation/faa-h-8083-21.pdf), [retrieved 11 October 2023].
- [4] Rolls-Royce plc, “M250-C20B training manual: Flight and engine controls,” 2018.
- [5] Swanda, A. P., and Seborg, D. E., “Controller performance assessment based on setpoint response data,” *Proceedings of the 1999 American Control Conference (Cat. No. 99CH36251)*, IEEE, 1999, 3863-3867 vol.6.
- [6] Lunze, J., *Regelungstechnik 1. Systemtheoretische Grundlagen, Analyse und Entwurf einschleifiger Regelungen*, 12th edn., Springer Berlin Heidelberg; Springer Vieweg, Berlin, Heidelberg, 2020.
- [7] Kyle Webb, *ESE 499 – Feedback Control Systems*, 2017.
- [8] Preiß, A., *Eintrittsstörungen bei Fluggasturbinen unter besonderer Berücksichtigung instationärer Gaszusammensetzungen*, 2001.
- [9] Arturo Urquiza, “PID controller overview,” [https://en.wikipedia.org/wiki/Closed-loop\\_controller#/media/File:PID\\_en.svg](https://en.wikipedia.org/wiki/Closed-loop_controller#/media/File:PID_en.svg).
- [10] Ang, K. H., Chong, G., and Li, Y., “PID control system analysis, design, and technology,” *IEEE Transactions on Control Systems Technology*; Vol. 13, No. 4, 2005, pp. 559–576. doi: 10.1109/TCST.2005.847331.

- [11] Jamsa-Jounela, S.-L., Poikonen, R., Georgiev, Z., Zuehlke, U., and Halmevaara, K., “Evaluation of control performance: methods and applications,” *Proceedings of the International Conference on Control Applications*, IEEE, 2002, pp. 681–686.
- [12] O'Connor, N., and O'Dwyer, A., “Control loop performance assessment: a classification of methods,” 2004.
- [13] *2018 5th International Conference on Signal Processing and Integrated Networks (SPIN)*, IEEE, 2018.
- [14] Boning, D. S., and Mozumder, P. K., “DOE/Opt: a system for design of experiments, response surface modeling, and optimization using process and device simulation,” *IEEE Transactions on Semiconductor Manufacturing*; Vol. 7, No. 2, 1994, pp. 233–244. doi: 10.1109/66.286858.
- [15] Guthrie, W. F., “NIST/SEMATECH e-Handbook of Statistical Methods (NIST Handbook 151),” 2020.
- [16] Alvarez, A. R., Abdi, B. L., Young, D. L., Weed, H. D., Teplik, J., and Herald, E. R., “Application of statistical design and response surface methods to computer-aided VLSI device design,” *IEEE Transactions on Computer-Aided Design of Integrated Circuits and Systems*; Vol. 7, No. 2, 1988, pp. 272–288. doi: 10.1109/43.3158.
- [17] Saravanamuttoo, H. I. H., Cohen, H., and Rogers, G. F. C., *Gas turbine theory*, 5th edn., Prentice Hall, Harlow, 2007.
- [18] Marcellan, A., Henke, M., and Schuldt, S., “A numerical investigation of the Water-Enhanced Turbofan laboratory-scale ground demonstrator,” *AIAA SCITECH 2022 Forum*, American Institute of Aeronautics and Astronautics, Reston, Virginia, 2022.
- [19] Krummrein, T., Henke, M., and Kutne, P., “A Highly Flexible Approach on the Steady-State Analysis of Innovative Micro Gas Turbine Cycles,” *Journal of Engineering for Gas Turbines and Power*; Vol. 140, No. 12, 2018. doi: 10.1115/1.4040855.
- [20] MacIsaac, B., and Langton, R., *Gas Turbine Propulsion Systems*, Wiley, 2011.

- [21] Bräunling, W. J., *Flugzeugtriebwerke*, Springer Berlin Heidelberg, Berlin, Heidelberg, 2015.
- [22] Mee, R., *A Comprehensive Guide to Factorial Two-Level Experimentation*, Springer New York, New York, NY, 2009.
- [23] Singh, R., Maity, A., and Nataraj, P. S., “Dynamic modeling and robust nonlinear control of a laboratory gas turbine engine,” *Aerospace Science and Technology*; Vol. 126, 2022, p. 107586. doi: 10.1016/j.ast.2022.107586.
- [24] Razak, A. M. Y., *Industrial gas turbines. Performance and operability*, CRC Press; Woodhead Pub, Boca Raton, Cambridge, England, 2007.
- [25] Landeshauptstadt Stuttgart, Amt für Umweltschutz, Abt. Stadtklimatologie, “Monatswerte 2023 - Messdaten der Station S-Mitte (Amt für Umweltschutz),” [https://www.stadtklima-stuttgart.de/index.php?klima\\_messdaten\\_download\\_afu](https://www.stadtklima-stuttgart.de/index.php?klima_messdaten_download_afu), [retrieved 7 November 2023].

# List of figures

FIG. 1. CROSS-SECTION VIEW OF THE M250-C20B [3].....	2
FIG. 2. INTEGRATION OF WET COMPONENTS INTO THE M250 ENGINE [1].....	3
FIG. 3. FEEDBACK CONTROL LOOP .....	5
FIG. 4. THE CONVENTIONAL CONTROL LOOP APPLIED TO THE M250-C20B [8] .....	6
FIG. 5. PID CONTROLLER STRUCTURE [9].....	7
FIG. 6. STEP RESPONSE OF A PID CONTROLLER (TRANSLATED) [6] .....	8
FIG. 7. PI CONTROLLER STRUCTURE [9].....	9
FIG. 8. RESPONSE TIME-DOMAIN CRITERIA. 1: $t_r$ , 2: $t_s$ , 3: OS .....	10
FIG. 9. GRAPHICAL ILLUSTRATION OF RESPONSE CURVE CRITERIA .....	12
FIG. 10. ILLUSTRATION OF FULL FACTORIAL DESIGN FOR THREE FACTORS .....	14
FIG. 11. ILLUSTRATION OF RSM DESIGNS FOR THREE FACTORS .....	16
FIG. 12 STRUCTURE OF THE SIMULINK® MODEL USED IN THE SIMULATION .....	21
FIG. 13. MODEL CONTROLLER BLOCK .....	21
FIG. 14. ALLISON M250 MODEL SYSTEM BLOCK .....	22
FIG. 15. M250 COMPRESSOR MAP WITH TRANSIENT OPERATION LINE [18] .....	23
FIG. 16. PARAMETER TABLE OF A PARAMETER STUDY .....	25
FIG. 17. APPLICATION OF THE FRAMEWORK IN THE M250 MODEL .....	26
FIG. 18. TRANSITION FROM GROUND TO FLIGHT IDLE.....	29
FIG. 19. PI-CONTROLLER BLOCK WITH OUTPUT SATURATION .....	30
FIG. 20. VARIATION OF N2 AS A FUNCTION OF TIME, $P_{el}$ AND $\Delta P_{el}$ .....	39
FIG. 21. COMPARISON OF THE TIME-DOMAIN .....	42

FIG. 22. RESPONSE CURVE CRITERIA COMPARISON.....	44
FIG. 23. 1 <sup>ST</sup> ORDER EFFECTS OF THE FULL FACTORIAL DESIGN USING ITAE CRITERION. ....	45
FIG. 24. INTERCEPTS FROM LINEAR REGRESSION .....	47
FIG. 25. FIRST ORDER MODEL AND REDUCED MODEL COMPARISON TO THE RESULTS OF THE FULL FACTORIAL.....	48
FIG. 26. COMPARISON OF RESPONSES FROM FIRST ORDER MODEL, SATURATED MODEL AND FROM AXIAL POINTS .....	49
FIG. 27. VARIATION OF THE POWER DEMAND AS A DISTURBANCE PARAMETER .....	51